The Journal of Physical Chemistry, Vol. 83, No. 3, 1979 379

Electron Spin Resonance Studies of Anisotropic Ordering, Spin Relaxation, and Slow Tumbling in Liquid Crystalline Solvents. 3. Smectics†

Wuu-Jyi Lin and Jack H. Freed*

Department of Chemistry, Cornell University, Ithaca, New York 14853 *(Received June 13, 1978)*

In this work the nonaxial ordering and spin relaxation of PD-Tempone spin probe in several liquid crystalline solvents exhibiting smectic A and B phases were studied utilizing methods previously employed by Polnaszek and Freed for the study of nematic liquid crystals. The results reported here for the isotropic and nematic phases are generally in accord with those obtained previously. An analysis of isotropic hyperfine shifts, changes in the ordering tensor, and anomalous relaxation behavior in the smectic phases suggest a model in which the PD-tempone probes are partially expelled from the dipolar region of the liquid crystalline molecules toward the more flexible hydrocarbon end chains as a result of the packing of the smetic layers, and concomitantly the probes increasingly experience a slowly relaxing local structure (SRLS) in a cavity-like location. Differences in observations from different types of smectic liquid crystals are interpreted in terms of their differing structures based on X-ray studies. It is shown that the angular dependent line widths in the smectic phases are significantly affected by the size and shape of the sample. These inhomogeneous broadening effects are discussed in detail in terms of static distortions of the smectic layering induced by wall effects and magnetic-field induced torques, and are in reasonable agreement with predictions of a simple model. The residual homogeneous widths are discussed in terms of combined models of anisotropic rotation and anisotropic viscosity as well as associated SRLS models. For the former case, the problem of defining the rotational diffusion tensor, which must be time dependent in any axis system, is discussed in some detail.

I. Introduction

In parts 1 and 2 we presented detailed studies of anisotropic ordering, line shapes, and relaxation for the weakly ordered perdeuterated 2,2,6,6-tetramethyl-4-piperidone *N*-oxide (PD-Tempone)[1] and the highly ordered cholestane (CSL) spin probe,[2] respectively, dissolved in nematic liquid crystalline solvents. In the present work we extend such studies to liquid crystalline solvents exhibiting smectic A and B phases.

There already exist a number of ESR studies of highly ordered spin probes in thermotropic liquid crystals exhibiting smectic phases.[3-7] However, as was pointed out in II, the use of such spin probes as CSL in these phases usually requires a "slow-tumbling" analysis if correct results on ordering and relaxation are to be obtained. With the exception of that work[2] (on the nematic phase) such analyses have not been employed. Therefore the analysis and interpretation of much of the previous work, based upon motional narrowing theory, is open to question.

We have chosen, in the present work, to concentrate on the PD-Tempone probe, which, because it is smaller and more weakly ordered, allows one to rigorously apply the simpler motional narrowing theory in most cases. We have already shown that the use of this radical offers the advantages that (1) one can achieve a high degree of spectral resolution for accurate spin-relaxation studies, because inhomogeneous broadening due to unresolved intramolecular proton or deuteron interactions is minimized; and (2) we now have extensive results in isotropic[8,9] and ordered phases[1,2,10,11] using this spin probe to serve as a basis for comparing and understanding new results in the smectic phases. We have indeed found that these two features enabled us to obtain new insights into the dynamical properties of these phases as monitored by the PD-Tempone probe.

An important feature in spin-relaxation studies in smectic phases is the ability to align the director in these phases by the applied dc magnetic field and to have the samples retain this alignment even when they are then rotated relative to the direction of the dc magnetic field[3-7] (i.e., "tilted"). Our results are consistent with this now familiar observation. However, largely because of the increased resolution, we found that the line widths and shapes will, in general, show angular-dependent effects which depend upon the size and shape of the sample. This feature, which was not fully considered in previous studies, must be adequately dealt with if meaningful studies of spin relaxation as a function of sample "tilt" angle are to be performed as discussed in this work.

II. Experimental Section

(A) *Preparation of Samples.* The liquid crystals *N*-(*p*-butoxybenzylidene)-*p*-*n*-octylaniline (40,8) and 4′-*n*-octyl-4-cyanobiphenyl (8CB) were purchased from Shawnee Chemical Co. and BDH Chemicals Ltd. respectively, while *N*-(*p*-butoxybenzylidene)-*p*-*n*-hexylaniline (40,6) was synthesized by condensing equimolar quantities of 4-*n*-butoxybenzaldehyde and 4-*n*-hexylaniline in absolute ethanol.[12] The molecular structures of these liquid crystals are shown in Figure 1. The 40,8 and 40,6 were purified by several recrystallizations from absolute ethanol till a constant melting point was achieved. The 8CB was used without further purification, since the transition temperatures were found to be in good agreement with published values. The nitroxide free radical, perdeuterated 2,2,6,6-tetramethyl-4-piperidone *N*-oxide (PD-Tempone), shown in Figure 2, was synthesized by standard methods[13] as previously discussed by Hwang et al.[8] Two sizes of cylindrical sample tubes were used for preparing the ESR samples: (1) 3 mm o.d., 2 mm i.d. pyrex and (2) 0.9 mm o.d., 0.5 mm i.d. capillary tubes. The radical solutions (5×10^{-4} to 10^{-4} M) were prepared by degassing on a vacuum line and were sealed off under a vacuum of 10^{-4} torr.

(B) *ESR Spectrometer.* The ESR measurements were performed on a Varian E-12 spectrometer using 10-kHz field modulation. The temperature in the active region of the cavity was controlled by a Varian E-257 variable temperature control unit to a long term stability of ±0.1 °C. The other aspects of the experimental methods are as described earlier.[1,8,10]

(C) *Aligning the Director in the Liquid Crystal Phases.* The sample was first heated to the isotropic or nematic

†Supported by NSF Grant DMR 77-17510.

0022-3654/79/2083-0379$01.00/0

ACRONYM	NAME	STRUCTURE
(4O,6)	N-(p-butoxybenzylidene)-p-n-hexylaniline	
(4O,8)	N-(p-butoxybenzylidene)-p-n-octylaniline	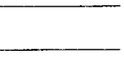
8CB	4-cyano-4'-octylbiphenyl	
MBBA	N-(p-methoxybenzylidene)-p-butylaniline	
CBOOA	N-p-cyanobenzylidene-p-octyloxyaniline	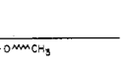
BOCP	bis(4'-n-octyloxybenzal)-2-chloro-1,4-phenylenediamine	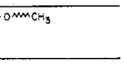
BEPC	butyl-p(p-ethoxyphenoxycarbonyl)-phenyl carbonate	
EMBAC	Ethyl-[(methoxybenzylidene)-amino] cinnamate	
phase V	mixture of four compounds	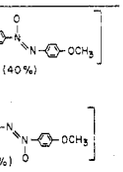

Figure 1. The structures of some liquid crystals discussed in this work.

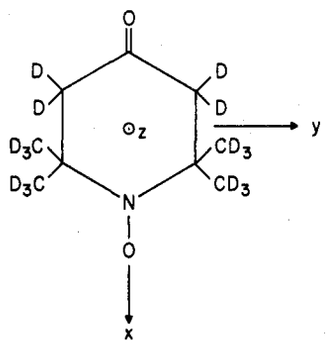

Figure 2. Perdeuterated 2,2,6,6-tetramethyl-4-piperidone *N*-oxide (PD-Tempone) showing the principal axis system for the magnetic tensors.

phase, while in the cavity of the E-12 spectrometer with a 3-kG magnetic field. In the nematic phase, the director is aligned parallel to the magnetic field of the spectrometer. The field was then increased to 13.5 kG and the sample temperature was slowly and carefully lowered until the smectic A phase was formed. This procedure was cycled a few times near the nematic–smectic A phase transition region. By this procedure the director was aligned in the S_A phase. With the exception of 8CB in the 2-mm tube, the director remained fixed in the sample independent of whether the sample tube was rotated in the high field. Also, the sample retained a fixed alignment through the S_B phase (under 3 kG) when the S_B phase was prepared by carefully lowering the sample temperature from the S_A phase which had previously been aligned as described. ESR spectra taken from samples from each phase prepared in this manner were reproducible with respect to even the finest details. (Note, however, that by gradually warming a sample from the S_B phase to the S_A phase [at 3 kG field] the ESR spectra for S_A were nearly, but *not* exactly, identical those prepared as given above, even though such a procedure lead to a set of reproducible spectra. Such matters are discussed further in section IIIF.) Also, it was found that this reproducibility was not affected as long as the magnetic field used for aligning the S_A phase was greater than about 8 kG.

(D) *Line Width Measurements.* All line width measurements were performed with the modulation amplitude set at a value of less than one-tenth of the line width and with the microwave power set well below that required to maximize the signal amplitude. The inhomogeneous deuteron broadening causes the line shapes to be non-Lorentizian and to appear to be broader than the true derivative peak-to-peak line width: $2|\gamma_e|T_2^{-1}(3)^{-1/2}$. The correct line width can be obtained[1,8] as follows: One accurately measures the line shape by noting the variation of the derivative half-amplitudes as a function of distance from the center. This line shape is then compared to a theoretical line shape calculated using an estimated intrinsic derivative peak-to-peak line width and hyperfine splitting constant for the deuterons causing the inhomogeneous broadening. The data collection and comparison with predicted line shapes was performed on-line with a minicomputer to yield values for $\langle a_D \rangle$ and intrinsic line widths for all three lines for each temperature. Some typical simulations for determining $\langle a_D \rangle$ in the S_A and S_B phases were also determined, where possible, by such a computer-assisted comparison. Typical values of $\langle a_D \rangle$ in different phases of 40,6 are given in Table I. Actually, once $\langle a_D \rangle$ is determined in this manner, it is usually more accurate to determine one line width, and then use the relative derivative amplitudes of the three lines to accurately determine the relative intrinsic widths of these lines.[1,8] The three intrinsic line widths are fitted to the equation

$$T_2^{-1}(M_I) = A + BM_I + CM_I^2 \qquad (1)$$

where M_I is the Z component of the ^{14}N nuclear spin quantum number, to obtain the coefficients A, B, and C.

It is not really necessary to determine $\langle a_D \rangle$ at every temperature studied, but rather it is sufficient to interpolate between a small set of such measurements for each phase, because (1) $\langle a_D \rangle$ does not change very much with temperature, and (2) the corrections to the line shape from the deuteron inhomogeneous broadening are not very great. We normally did not encounter any difficulties in determining $\langle a_D \rangle$ for the 0° tilt angle of the magnetic field. Measurements of the angular variation of $\langle a_D \rangle$ did indeed pose difficulties and will be discussed in section IIID. The theoretical basis for the angular variations is given in Appendix A.

TABLE I: Values of $\langle a_D \rangle$ in Different Phases of (40,6) from Line Shape Analyses

phase	θ, deg	$\langle a_D \rangle$,[a] mG	est $\langle a_D \rangle$,[b] mG
isotropic		−22.9 ± 0.6	
nematic		−17.6 ± 0.4	
S_A	0	−14.5 ± 0.3	−14.5
	22.5	−16.8 ± 0.4	−17.4
	45	−20.5 ± 0.1	−22.9
	67.5	−25.8 ± 0.3	−27.3
	90	−29.0 ± 0.2	−29.0
S_B	0	−22.4 ± 0.2	−22.4
	22.5	−21.7 ± 0.1	−24.4
	45	−23.7 ± 0.6	−28.7
	67.5	−29.1 ± 0.8	−32.5
	90	−33.9 ± 0.1	−33.9

[a] These results are virtually independent of temperature within each phase. They are for 0.5-mm i.d. samples. [b] These are estimated from the expression $\langle a \rangle = (\tilde{a}_\parallel^2 \cos^2\theta + \tilde{a}_\perp^2 \sin^2\theta)^{1/2}$ where $\tilde{a}_\parallel$ and $\tilde{a}_\perp$ are first determined from the results for $\langle a \rangle$ at 0 and 90°, respectively.

III. Results and Discussion

(A) *Magnetic Parameters.* The rigid limit spectra of PD-Tempone at −152 °C in the different solvents were recorded in order to obtain the magnetic parameters. The parameter A_z was easily determined from the spectrum. Since the ratio of A_z/a_N (where a_N is the isotropic hy-

TABLE II: Magnetic Parameters for PD-Tempone in Liquid Crystals[a,b]

		40,6 and 40,8				8CB		
	phase V[c]	isotropic	nematic	smectic A	smectic B	isotropic	nematic	smectic A
A_x, G	5.61 ± 0.2	5.58	5.56	5.54	5.51	5.54	5.52	5.50
A_y, G	5.01 ± 0.2	4.99	4.97	4.95	4.92	4.96	4.94	4.92
A_z, G	33.7 ± 0.3	33.5 ± 0.3	33.4	33.3	33.1	33.3 ± 0.3	33.1	33.0
$\langle A \rangle$,[d] G	14.77 ± 0.3	14.69	14.64	14.60	14.51	14.60	14.52	14.47
a_N, G	14.78 ± 0.02	14.70 ± 0.02	14.64	14.59 ± 0.02	14.50 ± 0.02	14.60 ± 0.02	14.54	14.49 ± 0.02

[a] Error limits are given for the experimentally determined values of the hyperfine interaction. All other values have been obtained by scaling as described in the text. [b] All measured g values were $g_s = 2.00602 \pm 0.00001$, so the **g** tensor determined for phase V (cf. ref 1) was used in all cases: $g_x = 2.0099 \pm 0.0002$; $g_y = 2.0062 \pm 0.0002$; $g_z = 2.00215 \pm 0.0001$. [c] From ref 1. [d] $\langle A \rangle \equiv {}^1/_3(A_x + A_y + A_z)$.

perfine constant) in the liquid crystals we studied (40,8, 40,6, 8CB) was found to be the same as in phase V,[1] and their absolute values are very close (cf. Table II), the other magnetic parameters A_x, A_y were simply scaled by the same factor of a_N(L.C.)/a_N(phase V) for the isotropic phase. In the S_A and S_B phases, the director was "locked-in" by the high field as stated previously, so the "isotropic" values of a_N in these phases could be obtained from the measurement of the angular dependence of $\langle a \rangle$. The angular dependence of the hyperfine coupling is given by (cf. Appendix A, eq A12):

$$\langle a \rangle = [\tilde{a}_{\parallel}^2 \cos^2 \theta + \tilde{a}_{\perp}^2 \sin^2 \theta]^{1/2} \cong a_N + {}^1/_2\chi(3 \cos^2 \theta - 1) \quad (2a)$$

where

$$\chi = (a_z - a_N)\langle \boldsymbol{D}^2_{00} \rangle_z - (1/\sqrt{6})(a_x - a_y)\langle \boldsymbol{D}^2_{20} + \boldsymbol{D}^2_{-20} \rangle_z \quad (2b)$$

and the approximate equality is for small χ (due to weak ordering) as is the case for PD-Tempone. We found from the results that the a_N values in the S_A and S_B phases are slightly smaller than those for the isotropic phase. This could be explained simply as follows: the PD-Tempone is gradually expelled by the liquid crystal molecules to the flexible end chain region, a matter to be discussed in detail shortly. Therefore the magnetic parameters in these phases were further scaled in the same manner as above. For the nematic phase, the director follows the 3-kG magnetic field, so we took a mean of the values for the isotropic and smectic A phases.

The isotropic g_s values of PD-Tempone in different phases was determined in the same way (cf. eq A12b). The isotropic g_s value was found to be constant $g_s = 2.00602 \pm 0.00001$ in all phases, and this is the same value as that for phase V solvent. We therefore concluded that the g values and most likely the **g** tensor is insensitive to any variation in environment in the liquid crystalline solvents, and we used the **g** tensor values previously obtained for phase V.[1] Figure 4 shows the very good agreement between theory and experiment for the angular dependences of $\langle a \rangle$ and $\langle g \rangle$ in the different phases and different solvents. The experimental results were identical for 40,6 and 40,8 no matter whether 2- or 0.5-mm i.d. samples were used. However, since 2-mm i.d. samples of 8CB followed the field, they gave no angular variation of $\langle a \rangle$ or $\langle g \rangle$. Table II gives the magnetic parameters we used for 40,6, 40,8, and 8CB. In order to develop a basis for understanding the variations of a_N (and also a_D, cf. Table I) with the phase as well as the solvent, we sought to develop good empirical relations between a_N (and a_D) and some measure of solvation effects.

A number of methods have been developed for estimating the polarity of solvents, and they have been reviewed and compared.[14,15] It is pointed out that the polarity of a solvent depends on a variety of intermolecular

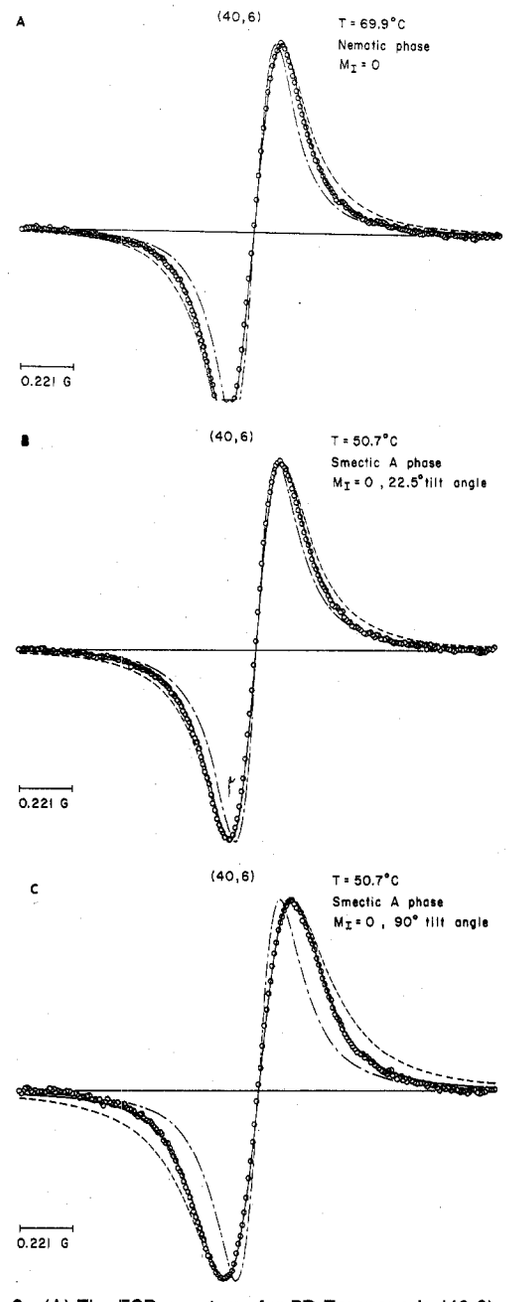

Figure 3. (A) The ESR spectrum for PD-Tempone in (40,6) nematic phase. The experimental points are represented by circles, the solid line is the best computer fit to the experimental data by adjusting the intrinsic width and a_D. The dashed line is a simple Lorentzian with the observed line width and $a_D = 0$. The broken line (- - - -) is a simple Lorentzian with the intrinsic line width and $a_D = 0$. (B) The ESR spectrum for PD-Tempone in (40,6) smectic A phase at 22.5° tilt angle of director with respect to the applied magnetic field. Other aspects as in A. (C) The ESR spectra for PD-Tempone in (40,6) smectic A phase at 90° tilt angle of director with respect to the applied magnetic field. Other aspects as in A.

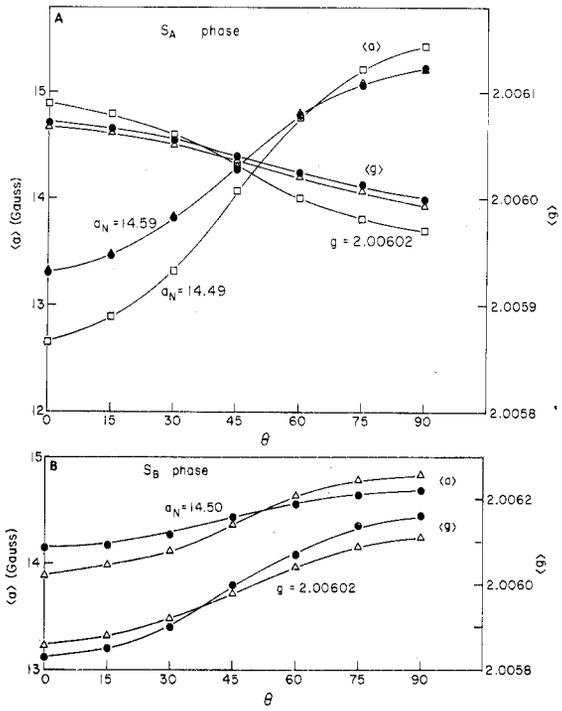

Figure 4. (A) The angular dependence of $\langle a \rangle$ and $\langle g \rangle$ in the smectic A phases of (40,6), (40,8), and 8CB for PD-Tempone. Solid circles are for (40,6) at $T = 50.7$ °C; open triangles are for (40,8) at $T = 63.8$ °C; open squares are for 8CB at $T = 28.6$ °C. The curves are the theoretical prediction from eq 3. For (40,6) and (40,8) these results are independent of whether 2- or 0.5-mm sample tubes were used. (B) The angular dependence of $\langle a \rangle$ and $\langle g \rangle$ in the smectic B phases of (40,6) and (40,8) for PD-Tempone. The solid circles are for (40,6) at $T = 34.5$ °C and open triangles are for (40,8) at $T = 47.0$ °C. These results are independent of whether 2- or 0.5-mm sample tubes are used.

forces as well as hydrogen bonding between the solvent and the solute. The idea of the empirical methods is to use a particular solvent-dependent standard process. The most comprehensive solvent scale given[14] is the E_T or molar transition energy scale based upon the use of pyridinium *N*-phenolbetaine, which gives a very large displacement of the solvatochromic band in different solvents (E_T (kcal/mol) $\equiv 2.86 \times 10^{-3}\tilde{\nu}$ where $\tilde{\nu}$ is the absorption maximum in cm^{-1}). We have found the E_T scale very useful for representing solvent variation of a_N (and a_D). This is shown in Figure 5. The basis of the linear relationships between a_N (and a_D) and E_T are the six or seven solvents for which both E_T has been determined,[14,18] and we have measurements of a_N and a_D. Only in the case of water solvent was there a large discrepancy with the linear relation from the other solvents. This is not surprising given the very unique properties of water as a solvent. Thus we chose to redefine the E_T value appropriate for PD-Tempone in water. The E_T values for the other solvents, in particular the liquid-crystalline solvents, were then determined using this graph. It is interesting to note that we generally find good agreement between the E_T determined from the a_N and that determined (but with less sensitivity or accuracy) from a_D. The general (and well-known) trends are for a_N to increase with increasing solvent polarity while a_D decreases (e.g., solvent complexing with >N÷O is enhancing the unpaired electron density at the N÷O site).

Previous workers[16] have related solvent polarity shifts of a_N in spin labels largely to dielectric effects, but these other methods do not adequately account for hydrogen bonding.[17] However, this appears to be no problem for the empirical E_T values (cf. Figure 5) with the exception of water. Results like ours in Figure 5 can easily be extended

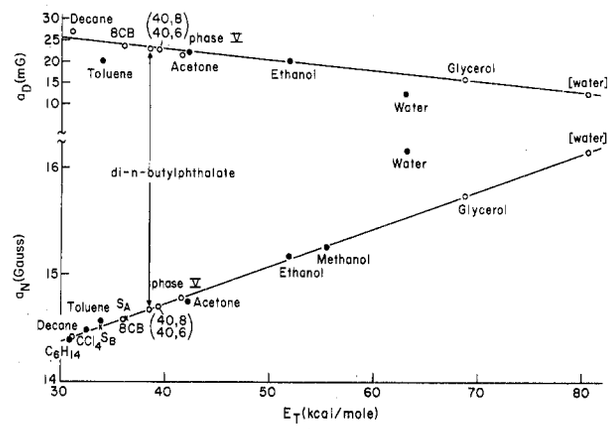

Figure 5. The experimentally determined variation of a_N and a_D for PD-Tempone with E_T (the molar transition energy scale)[14] in different solvents. The straight lines are drawn through the experimental data represented by the solid circles, corresponding to those solvents for which E_T has been independently determined. (Water is an exception.) For those solvents for which E_T data are not available, we show the experimental a_N values on this straight line by open circles, and this sets the E_T value. The a_D values were then plotted using these results for E_T. The S_A and S_B phases in (40,6) or (40,8) are represented by a cross.

to a variety of spin probes in many solvents to establish useful empirical relations for variation of a_N (as well as proton and deuteron "a" values) with solvent.

We note in all cases the decrease in a_N in going from the isotropic → nematic → smectic A → smectic B phases. One expects, from Figure 5, that this decrease will correlate with a changing "effective" location of the PD-Tempone such that it is gradually expelled from the region where it is in proximity to the dipolar portions of the liquid crystal molecules to regions where it is in greater proximity to the hydrocarbon chains (e.g., the typical a_N for the isotropic phases of the liquid crystalline solvents is close to that for acetone or di-*n*-butylphthalate,[9] while in smectic B it is approaching that of decane[9]). One expects an increased packing with the lower temperature phases. Thus, while the PD-Tempone, with a dipolar end, might prefer a location closer to the dipolar region of the solvent molecules, it can probably find more available space in regions of the flexible hydrocarbon chains as the packing of the liquid crystalline molecules becomes denser.

(B) *Order Parameters and Potential Expansion Coefficients.* (1) *Results.* The $\langle a \rangle$ and $\langle g \rangle$ values in the different phases for different solvents are shown in Figure 6. The results for 40,6 and 40,8 are quite similar (but not identical). This is to be expected considering their very similar structures. Following I the two-term order parameters can be calculated from the equations[1] (see also Appendix A):

$$\langle \boldsymbol{D}^2_{00} \rangle_z = \frac{(\langle a \rangle - a)(g_x - g_y) - (\langle g \rangle - g)(a_x - a_y)}{(a_z - a)(g_x - g_y) - (g_z - g)(a_x - a_y)} \tag{3a}$$

$$\langle \boldsymbol{D}^2_{20} + \boldsymbol{D}^2_{-20} \rangle_z = \frac{\sqrt{6}[(\langle a \rangle - a)(g_z - g) - (\langle g \rangle - g)(a_z - a)]}{(g_x - g_y)(a_z - a) - (g_z - g)(a_x - a_y)} \tag{3b}$$

(where we have dropped the subscript on a_N). The subscript z on the order parameters indicates that they are referred to the magnetic z axis of PD-Tempone as the primary reference axis. If the magnetic tensor y axis is taken as the primary reference axis, then one may calculate $\langle \boldsymbol{D}^2_{00} \rangle_y$ and $\langle \boldsymbol{D}^2_{20} + \boldsymbol{D}^2_{-20} \rangle_y$ from eq 3 after first performing the permutations $z \rightarrow y \rightarrow x \rightarrow z$. [Note that $\sum_{i=x,y,z} \langle \boldsymbol{D}^2_{00} \rangle_i = 0$ and $\sum_{i=x,y,z} (\langle \boldsymbol{D}^2_{20} \rangle_i + \langle \boldsymbol{D}^2_{20} \rangle_i) = 0$.] We

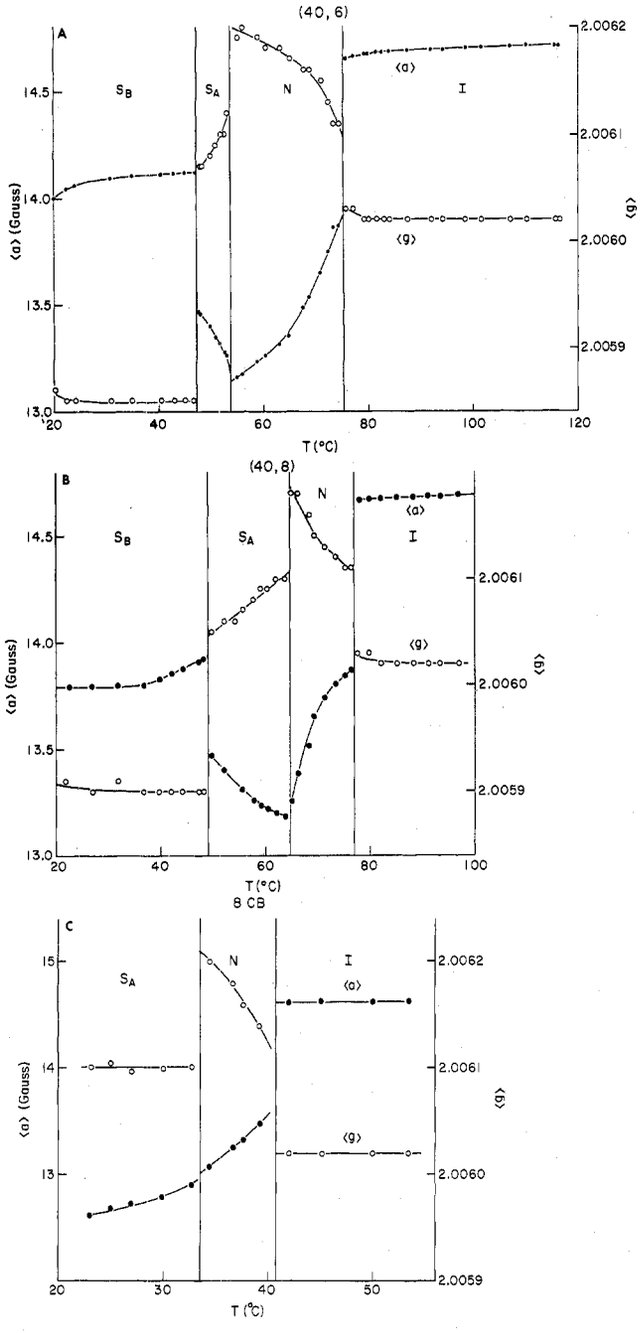

Figure 6. The variation of $\langle a \rangle$ and $\langle g \rangle$ with temperature for PD-Tempone in (A) (40,6), (B) (40,8), (C) 8CB. The solid circles are for $\langle a \rangle$ and the open circles are for $\langle g \rangle$.

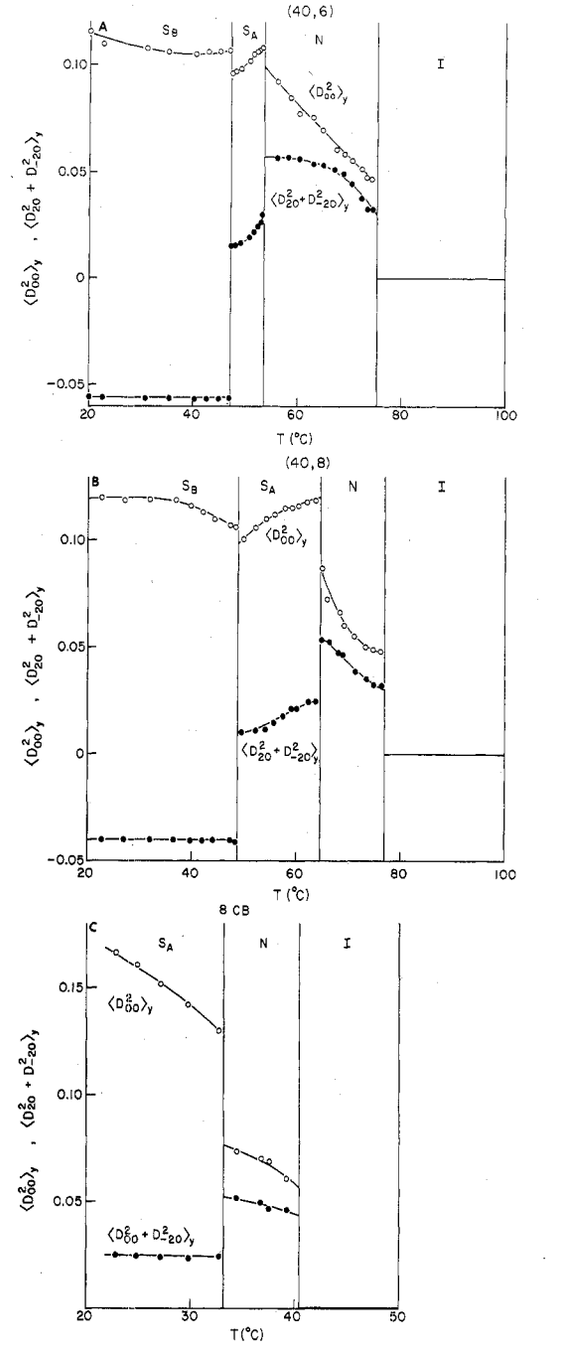

Figure 7. The variation of the order parameters with temperature $\langle D^2_{00} \rangle_y$ (open circles) and $\langle D^2_{20} + D^2_{-20} \rangle_y$ (closed circles) for PD-Tempone in the different phases of (A) (40,6), (B) (40,8) and (C) 8CB.

show the y ordering vs. temperature for the different liquid crystals in Figure 7. The results for 40,6 and 40,8 show similar temperature dependences, i.e., the ordering is almost constant in the S_B phase, increasing gradually with increasing temperature in the S_A phase, and decreasing in the nematic phase. The same type of temperature dependence of order parameter ($\langle D^2_{00} \rangle$) has been observed in EMBAC (cf. Figure 1) by NMR methods.[5] Note that the ordering is nearly axially symmetric about the molecular y axis in the smectic phases, but there is a non-negligible nonaxial $\langle D^2_{20} + D^2_{-20} \rangle$ in the S_B, which changes sign in the S_A phase and becomes almost negligible The angular-dependent results for $\langle a \rangle$ and $\langle g \rangle$ in the smectic B phase in 40,6 and 40,8 shown in Figure 4B, as well as the very good alignment of these phases is consistent with this phase being B_A (and not B_c).[5] We are not aware of a previous determination of the symmetry of this phase for these smectics.

In the S_A phase of 8CB, $\langle D^2_{00} \rangle$ decreases with increasing temperature, which is the reverse of the behavior of 40,6 and 40,8. Note that in Figure 6 there are hints of pretransitional effects in the isotropic phase just at the I → N phase transition (see below).

In order to perform relaxation studies, one must know the coefficients in the potential which determines the distribution function for the orientation of PD-Tempone. As in I we used the two term ordering tensor defined by

$$\langle D^2_{K0}(\Omega) \rangle = \int d\Omega \, P_{eq}(\Omega) \, D^2_{K0}(\Omega) \qquad (4a)$$

where Ω represents the Euler angles between the molecular coordinate system and the laboratory system, and $P_{eq}(\Omega)$ the equilibrium distribution function given by

$$P_{eq}(\Omega) = \exp(-U(\Omega)/kT) / \int d\Omega \exp(-U(\Omega)/kT) \qquad (4b)$$

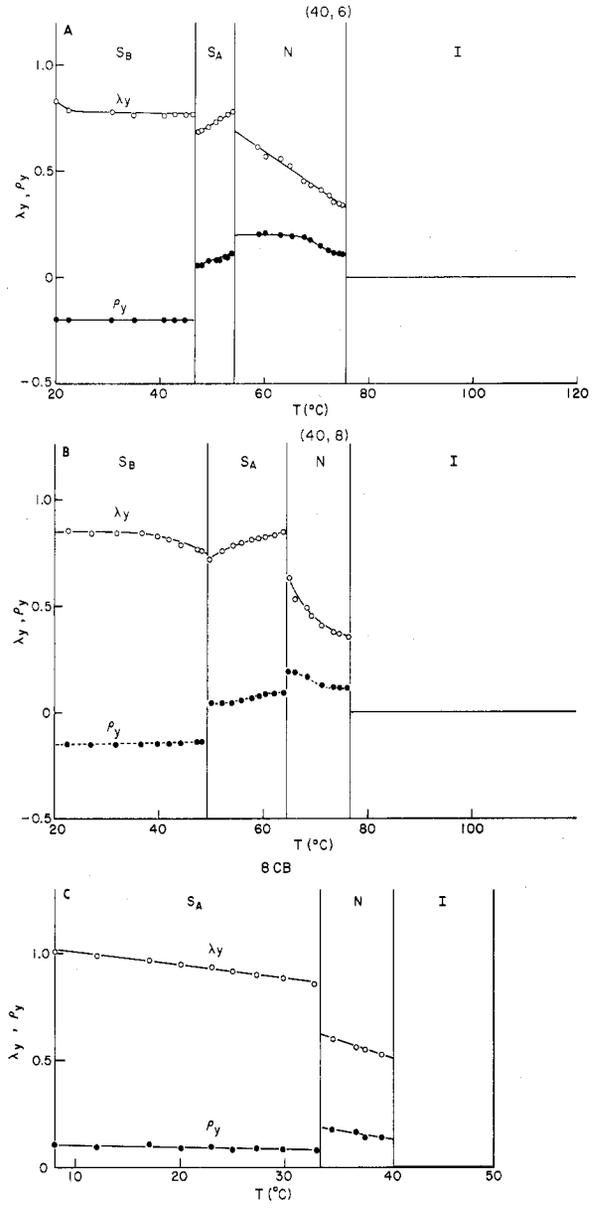

Figure 8. The asymmetric ordering parameters λ_y and ρ_y vs. temperature for PD-Tempone in the different phases of (A) (40,6), (b) (40,8), and (C) 8CB. The open circles are for λ_y, the closed circles are for ρ_y.

where $U(\Omega)$ is the mean restoring potential for PD-Tempone in the field of nematic solvent molecules, which we approximate with two terms:

$$U(\alpha,\beta,0)/kT \simeq -\lambda \cos^2\beta - \rho \sin^2\beta \cos^2\alpha \quad (5)$$

The coefficients λ and ρ are obtained, via this set of equations, from the results on $\langle \boldsymbol{D}^2_{00} \rangle$ and $\langle \boldsymbol{D}^2_{20} + \boldsymbol{D}^2_{-20} \rangle$, and they are shown in Figure 8 vs. temperature for the different solvents.

(2) *Discussion of Order Parameters.* Before attempting to explain the opposite trends in PD-Tempone ordering vs. temperature for the S_A phases of 40,8 and 40,6 on the one hand and 8CB on the other, it is useful to consider differences between them as found from X-ray studies on related liquid crystals.[18] In most liquid crystals, the polar segments of the molecules are in the middle with hydrocarbon chains extending outward (e.g., 40,6 and 40,8, cf. Figure 1). This type of molecule tends to form monolayer S_A phases, and the lamellar thickness is typically equal to or slightly less than the molecular length, presumably due to a slight interpenetration of the layers, and/or to departures of the hydrocarbon chains from their fully extended conformations. However, certain cyano Schiff bases and cyanobiphenyls with alkyl or alkoxy end groups such as 8CB (cf. Figure 1) are found to exhibit a bilayer type of S_A phase, where the lamellar spacing is about 1.5 times the molecular length. This is believed due to the fact that these molecules each have a polar and a long-chain nonpolar end and must adjust to the tendencies of these groups to interact with similar groups. When the temperature is lowered, the first type of liquid crystal (40,6; 40,8) exhibits a decrease in its interlamellar spacing, while the second type (8CB) exhibits an increase. The type 1 contraction is expected as the thermal motions of the hydrocarbon chains decrease, so the packing forces are more effective. The type 2 expansion must be due to a tendency of the like ends of the molecules to draw closer, a process that is prevented by the interdigitated bilayer arrangement of this S_A phase. (In fact it has been observed that some type 2 liquid crystals not only experience an increase in the interlamellar spacing with increased pressure, but also yield a "re-entrant" nematic phase by super-cooling the S_A phase, in order to achieve an energetically more favorable packing[19]).

Thus the PD-Tempone molecule, which appears to be gradually expelled (with decreasing temperature) from the highly ordered polar region to the less ordered hydrocarbon regions might be expected to exhibit decreased average ordering as the flexible end chains interpenetrate more, and their dynamical motions interfere with their ordering. Further aspects of this model are discussed below in the context of the spin relaxation results. [Note that a highly ordered spin probe such as CSL appears to show increasing order with decreasing temperature in the S_A phase[4] (but this result has yet to be corrected for slow tumbling effects), most likely because this large molecule is ordered so as not to be affected much by the effects of the end chain flexibility, and instead it experiences the increased ordering of the central polar portion of the liquid crystal molecules as the temperature is reduced.] Now, in the case of 8CB, the hydrocarbon chains should experience reduced packing with decreased temperature, so the site occupied by the PD-Tempone shows less interference, and its ordering increases more naturally with decreased temperature.

Furthermore, let us note that for all three liquid crystals the PD-Tempone exhibits very nearly axially-symmetric ordering about its molecular y axis (cf. Figure 2) in the S_A phase, while this was not the case in the nematic. This observation is consistent with our model involving the expulsion of PD-Tempone toward the flexible hydrocarbon chains and its experiencing random ordering fluctuations along its x–z plane (that is paralled to the smectic layers), which have a near-zero net average. (This point is not really strictly sound because the smectic layering is parallel to the smectic x''–y'' plane, and only because of the partial ordering of the PD-tempone is its molecular x–z plane *partially* aligned parallel to the smectic x''–y'' plane.)

The changes in PD-Tempone ordering in going from $S_A \rightarrow S_B$ appear to suggest (1) that the degree of ordering in the two phases is comparable; but (2) there is somewhat larger anisotropy of ordering in the x–z plane probably due to decreased flexible motion of the hydrocarbon chains which might otherwise tend to average out such ordering. This is discussed further below.

One might wish to interpret the pretransitional effects that appear for $\langle a \rangle$ and $\langle g \rangle$ (cf. Figure 6), in terms of the quasi-critical fluctuations in ordering in the isotropic phase near the I $\rightarrow$ N phase transition. One finds from Lan-

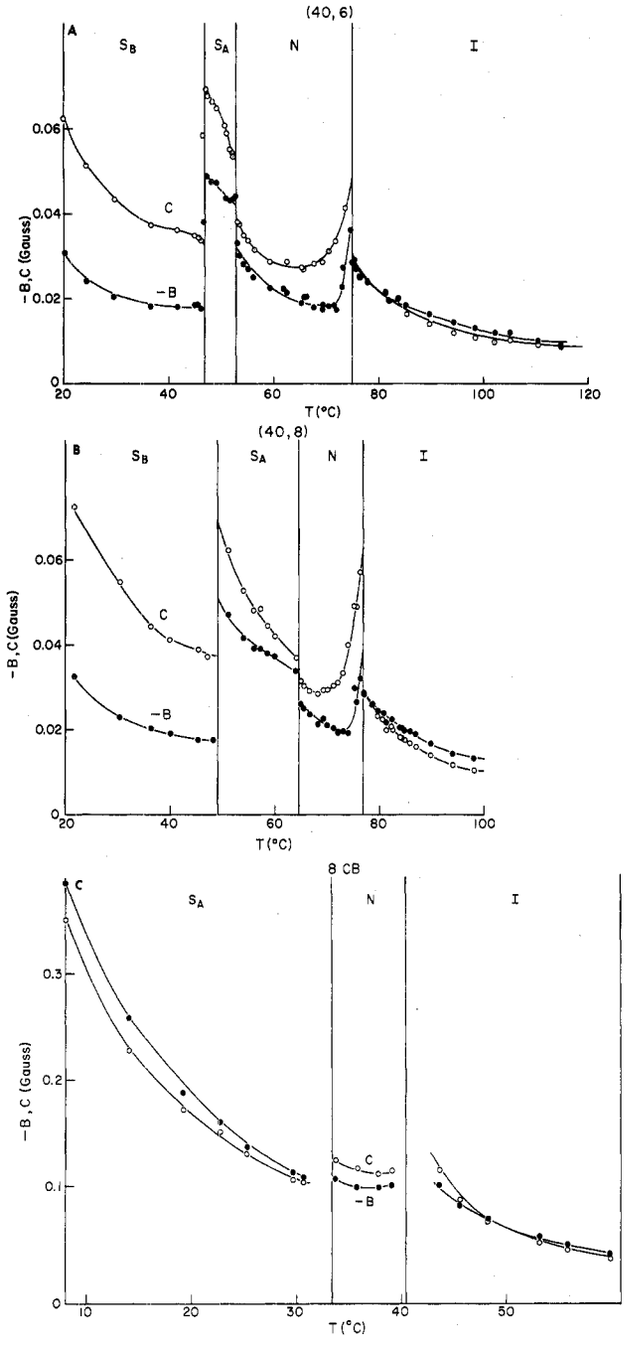

Figure 9. The variation of $-B$ and C with temperature in (A) (40,6), (B) (40,8), and (C) 8CB. The closed circles are for $-B$ while the open circles are for C.

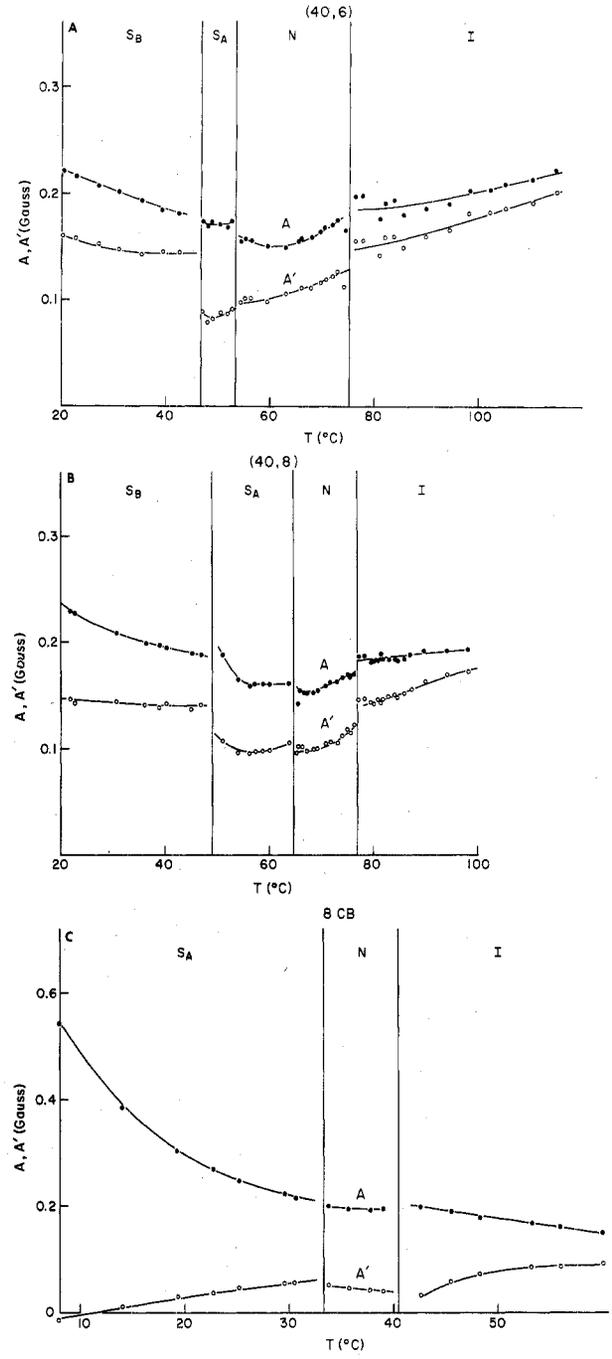

Figure 10. The variation of A and A' with temperature in (A) (40,6), (B) (40,8), and (C) 8CB. The residual A' was calculated using an anisotropic rotation model.

dau–deGennes mean-field theory[20] that there is a non-zero order parameter $S^{(s)}$ for the liquid crystalline solvent which obeys the following expansion as a function of magnetic field strength B:

$$S^{(s)}(B) = \eta B^2 + \text{H.O.T.} \tag{6a}$$

where

$$\eta \equiv \left.\frac{\partial S^{(s)}}{\partial B}\right|_{B^2=0} = \frac{2\chi_a}{9a(T - T_c^*)} \tag{6b}$$

is the "paranematic susceptibility", χ_a is the anisotropy in the diamagnetic anisotropy, T_c^* is the "apparent" critical T, and a is the appropriate mean-field constant. With typical estimates of $a \sim 4 \times 10^5$ erg/K cm^3, $T - T_c^* \sim 1$ °C, $\chi_a \sim 10^{-6}$ cgs, and $B \sim 3.3$ kG, one gets $S^{(s)} \sim 5 \times 10^{-6}$ or an effect much too weak to see. Now η may be directly related to the phenomenon of magnetic birefringence[20] which has been carefully studied by light scattering, yielding experimental results in complete agreement with the mean-field theory. Thus, it is quite clear that our ESR observations cannot be interpreted in terms of such a small static $S^{(s)}$ (and hence an even smaller ordering of the probe). However, the dynamic effects of the quasi-critical fluctuations are now known to cause large ESR line width anomalies,[11] and usully associated with the line width contributions from the spin relaxation are the dynamic frequency shifts from the nonsecular and pseudosecular contributions.[1,8,21] It seems quite reasonable, therefore, to ascribe pretransitional effects on $\langle a \rangle$ and $\langle g \rangle$ to the *dynamic* frequency shifts in the ESR resulting from the quasi-critical fluctuations.

(C) *Line Width Analysis and Discussion.* The ESR spectra of PD-Tempone in these three solvents are all in the motional narrowing region. The line width coefficients

A, B, and C (cf. eq 1) vs. temperature are shown in Figures 9 and 10. We found that the line widths obtained for the isotropic, nematic, or S_A and S_B phases at 0° tilt angle are all independent of the sample size as one would normally expect. The significance of this observation will be explored in the next section.

We note in Figure 9 that in all cases in the isotropic phase the C and B parameters are nearly equal at a given T. This is the expected normal behavior for PD-Tempone in isotropic phases.[1,8] Near the isotropic–nematic phase transition there are clear indications of an anomalous increase in B and C, an effect which is more prominent on the nematic side, and has been related by Rao et al.[11] to quasi-critical fluctuations at this weak first-order transition. This effect obscures somewhat the nonanomalous portions of B and C in the nematic phase. These portions are perhaps clearest in the case of 40,6 showing a characteristic increase with decreasing temperature. The change from N to S_A is characteristically abrupt with no hint of any pretransitional effect, which could be due to a very narrow temperature range that shows quasi-critical behavior; but this has yet to be investigated. Notice in the S_A phases of 40,6 and 40,8 the C/B ratio is greater than one and appears to be increasing with decreasing temperature, but it is not much different from unity for 8CB. The transition from $S_A \rightarrow S_B$ again yields abrupt changes in B and C, and the S_B phase is characterized by (1) values of C and B which are markedly reduced from the higher temperature S_A phases, or the opposite of what is normally expected; and (2) ratios of $C/B \gtrsim 2$ which again are abnormal. The values of A are shown for all phases and solvents in Figure 10. The low temperature phases show characteristic increase in A with decrease in T, while the highest T regions show the reverse behavior, as is normally expected.[1,8]

Again we focus mainly on the B and C coefficients, which may be interpreted in terms of the rotational dynamics of the PD-Tempone in the (ordered) fluids. Our analysis is in accordance with the methods we have previously used.[1,8,10] (In particular, one used eq 2.28–2.31 of I.) We consider the phases separately, starting with the high temperature isotropic phases.

(1) *Isotropic Phase.* One finds that for PD-Tempone in the isotropic phase, one is in the region where nonsecular contributions to A, B, and C are expected to be important (i.e., $\omega_0^2\tau_R^2 \sim 1$). That is, for 40,6 and 40,8 the accessible range of rotational correlation time, τ_R, is about 10–30 ps, while for 8CB it is somewhat longer: 30–100 ps. We find just as in I, that the results can be interpreted either by employing some anisotropy for rotation about the molecular y axis (i.e., $N_y = 4.3 \pm 0.3$ for 40,6; $N_y = 3.8 \pm 0.2$ for 40,8; and $N_y = 1.4 \pm 0.2$ for 8CB), or else by correcting the nonsecular spectral density function to become $\tau_R/(1 + \epsilon\tau_R^2\omega_0^2)$, where the adjustable parameter $\epsilon \geq 1$, is believed to be indicative of deviation from simple Brownian rotational diffusion. The theory[8] for ϵ relates it to the finite lifetime of the fluctuating torques causing the rotational motion of the PD-Tempone. The results can all be "explained" with $N \simeq 1$ (which is typical of PD-Tempone in simple liquids) and $\epsilon = 10 \pm 2$ for 40,6, $\epsilon = 7 \pm 1$ for 40,8, and $\epsilon = 3 \pm 1$ for 8CB. The value for 8CB is in keeping with our previous results on isotropic phases, while those for 40,6 and 40,8 are somewhat greater. As we noted in I, it is not possible to distinguish between the contributions from the two sources from such data in the isotropic phase, because the I → N phase transition prevents studying lower temperature regions of the isotropic phase where the effects of ϵ are suppressed.[8] In I we adopted the

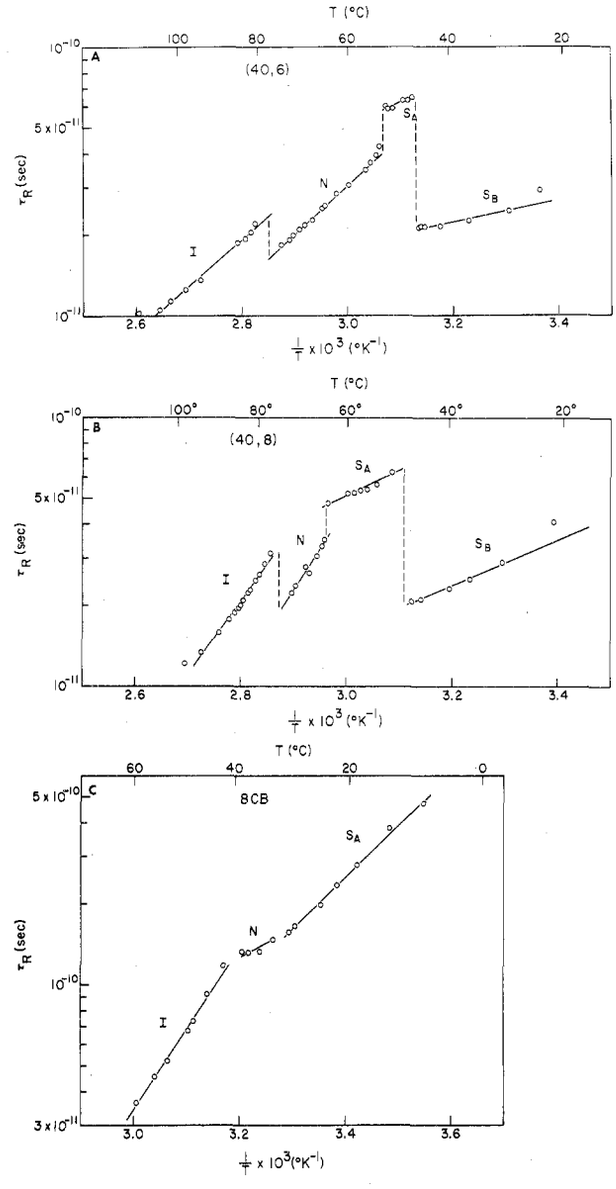

Figure 11. τ_R vs. $1/T$ for PD-Tempone in (A) (40,6), (B) (40,8), and (C) 8CB.

point of view of using $\epsilon \sim 4.5$ by comparison with other nonnematic[8] solvents. If we do that here we would then obtain ($N_y = 1.9 \pm 0.4$ for 40,8, $N_y = 1.6 \pm 0.2$ for 40,8, and $N_y = 0.97 \pm 0.36$ for 8CB). There was one case in I similar to our present observations on 40,6 and 40,8. It was for the solvent BEPC (cf. Figure 1) which yielded $N_y = 2.3 \pm 0.6$ for $\epsilon = 4.6$. The question of the "best" set of ϵ and N_y is discussed further below.

As before, the $\tau_{\bar{R}}$ values [$\bar{R} \equiv (R_\parallel R_\perp)^{1/2}$ and $\tau_{\bar{R}} \equiv (6\bar{R})^{-1}$ with $R_\parallel$ and $R_\perp$ the respective parallel and perpendicular components of the rotational diffusion tensor] are virtually the same for any of the sets of ϵ and N_y which fit the data. They are plotted in Figures 11 vs. $1/T$ and show the characteristic increase with decreasing T. The activation energies from these $\tau_{\bar{R}}$ values appear in Table III, and are found to be of the order expected for liquid crystal solvents (cf. I). The rather large difference in E_a between 40,8 and 40,6, despite their very similar molecular structure is, however, surprising.

A preliminary analysis of the A' results shown in Figure 10 in terms of the spin-rotational mechanism was made in the manner of Hwang et al[8]. (Note A' is that portion of A in eq 1 which remains after dipolar and **g** tensor contributions are substracted.) In that work it was shown

TABLE III: Activation Energies and Preexponential Factors for Rotational Relaxation of PD-Tempone Dissolved in Liquid Crystal and Related Solvents

solvent	phase	E_a,[d] kcal/mol	ln A,[d] (s)
(40,6)[a]	I	8.1 ± 0.2	−36.1 ± 0.3
	N	8.4 ± 0.4	−36.8 ± 0.7
	S_A	(4.2 ± 0.6)	(−29.1 ± 1.4)
	S_B	2.0 ± 0.3	−27.9 ± 0.5
(40,8)[a]	I	12.5 ± 1.1	−42.3 ± 1.6
	N	(13.7 ± 2.0)	(−44.5 ± 3.6)
	S_A	4.2 ± 0.7	−30.0 ± 1.2
	S_B	4.0 ± 0.3	−30.8 ± 0.5
8CB[a]	I	14.9 ± 0.1	−45.3 ± 0.2
	N	(4.1 ± 1.6)	(−29.3 ± 2.6)
	S_A	8.5 ± 0.4	−36.7 ± 0.6
phase V[b]	I	8.0	−37.6
	N	9.6	−38.9
BOCP[b]	N	9.4	−36.4
MBBA[b]	N	10.2	−39.5
(*n*-decane *n*-dodecane)[c]	I	3 to 5	
di-*n*-butylphthalate[c]	I	8.55	

[a] This work. [b] Reference 1. [c] Reference 9. [d] Results in parentheses are uncertain because of small temperature range of this phase.

that in the high temperature regions one expects $A' = A_1^2\tau_R^{-1}$ where A_1^2 is a constant equal to 5×10^{-13} G s from simple spin-rotation theory for the PD-Tempone g values. In normal liquids[8] it ranged from 6 to 10×10^{-13} G s, and was estimated as 15.7×10^{-13} G s for phase V.[1] At lower temperatures, the A' increases anomalously with τ_R, and this makes it difficult to obtain A_1^2 unless high enough temperature results are obtained. Unfortunately, we were limited in this respect, and estimated A_1^2 by fitting our data of the form $A'\tau_R^{-1} = A_1^2\tau_R^{-2} + A_2^2$ (where A_2^2 is the constant for the anomalous A' dependence upon τ_R at lower temperatures).[8] We obtained values for A_1^2 of 19.4, 17.8, and 29.1×10^{-13} G s for 40,6, 40,8, and 8CB, respectively. These are high and would tend to suggest large deviations from simple rotational diffusion theory. However, because of the difficulty in extracting A_1^2 from our results, they should be confirmed by T_1 measurements[8] before they are analyzed further.

(2) *Nematic Phase.* The nematic phase results require an analysis which includes reorientation in the potential field of the oriented solvent molecules. This was performed as in I utilizing the ordering terms λ and ρ in Figure 8. Actually, because of the narrow range of the nematic phases, especially in 40,8 and 8CB it was difficult to separate out quasi-critical effects associated with the N ↔ I phase transition from the "background" contributions to B and C which determine τ_R (this is particularly true for the C values of 40,8). In the best case, viz. 40,6, the lower temperature nematic results could be fitted to an $\epsilon = 4.5$ and $N_y \sim 2.5$ near the N → S_A transition and increasing to an $N_y \sim 4$ at higher T, but the residual contributions from the quasi-critical effects to this latter value remain uncertain until a more careful analysis[11] is made of them. For these slower motions ($\tau_R \approx 50$–60 ps), the use of an $\epsilon \sim 10$ yields N_y values only very slightly smaller than those obtained for $\epsilon \sim 4.5$ (i.e., about 0.2–0.3 less). Similar, but less definitive results are obtained for 40,8 and 8CB. We may note that in I the results for BEPC yielded an $N_y = 1.6 \pm 0.2$, while that for BOCP (which could not be studied in the isotropic phase) was $N_y = 9.4 \pm 1.5$. All other cases yielded $N_y \approx 1$. One can see from Figure 1 that BOCP has the longest hydrocarbon end chains of all liquid crystals shown (and the longest overall molecular length), with 40,6, 40,8, and 8CB somewhere in between BOCP and BEPC in this characteristic. This suggests some correlation between chain length and the estimated N_y values. (This correlation would be consistent with the explanation of these results in terms of the SRLS model that is discussed below.)

It was found in I for the case of the nematic solvents phase IV and phase V, that (even though $N_y = 1$), when $\tau_R > 10^{-10}$ s, there is an anomalous increase in $\tau_R(C)/\tau_R(B)$ from unity; (here $\tau_R(C)$ and $\tau_R(B)$ are the τ_R values estimated from the C and B line width parameters, respectively, with $N_y = 1$ unless stated otherwise). For the present solvents, the N → S_A phase transition prevented the achievement of such slow τ_R values in the nematic phase. For such slow motions, one had to consider the effects of the different models on the nonzero spectral densities (in particular the pseudosecular spectral densities). In that work the effects of (1) anisotropic rotation; (2) anisotropic viscosity; (3) fluctuating torques, and (4) slowly relaxing local structure (SRLS) were considered in detail and further elaborated in the pressure-dependent work of Hwang et al.[10] (This reference gives summaries of all these mechanisms.) It turns out that $\tau_R(B)$ is a good index of the correlation time of PD-Tempone for these models especially when nonsecular terms are not important. For model (2) anisotropic viscosity, one has $\tau_R(B) = \tau_{\hat{R}\perp}$; while for model (3) $\tau_R(B)$ is only affected by an ϵ'_s which was required to be close to unity while $\tau_R(C)$ is affected by $\epsilon'_{ps} \geq 1$ as well. For model (1) anisotropic rotational diffusion the predicted value of $\tau_R(B)$ is significantly less affected by varying N_y than is $\tau_R(C)$ (an example of this is given below). While for model (4), SRLS (when we restrict ourselves to τ_R values $< 10^{-10}$ s) there is a simple relation between the estimate of N_y and the estimate of the SRLS parameters as shown below. Thus, for convenience, we plot $\tau_R(B)$ values for all the ordered phases in Figure 11 (except as noted). We have used these $\tau_R(B)$ values as our best estimates of activation energies in these phases independent of our attempts at detailed analysis of the models. (The results in I and in Hwang et al.[10] were shown for models 2 and 3 corresponding to our present use of $\tau_R(B)$, as well as for model 1). One notes from Table III that the E_a values for the solvents 40,6 and 40,8 are a little increased in the nematic phases over their isotropic values (such was the case for phase V solvent, cf. 1.) The E_a value for 8CB appears to be markedly reduced, although its magnitude is highly uncertain because of the very limited temperature range of this phase. (A similar trend appears for the case of BEPC, cf. I.) These results suggest that the microscopic molecular dynamics are not markedly changed by the I → N transition (except perhaps for 8CB).

(3) *Smectic A Phase.* The results for the smectic A phases are somewhat easier to handle than were those for the nematic phases, because of the absence of any quasi-critical effects persisting into the phase. The results for 40,6 and 40,8 are quite similar with some differences for 8CB. There is an increase in τ_R values in passing through the N → S_A phase transition for 40,6 and 40,8. This is, however, associated with a large *decrease* in E_a for these solvents in the S_A phase. This appears contrary to what would be expected for the more viscous S_A phase. The ordering tensor for PD-Tempone was found to exhibit significant changes (cf. Figures 7 and 8 and section B) that reflect less the increased ordering expected for the S_A phase than the changed nature of the ordering of PD-Tempone. All these observations seem to support our point of view that the PD-Tempone is expelled more into the hydrocarbon regions of the smectic layers due to the smectic

packing (as compared to the nematic phase in which polar interactions of the > N÷O group with the central portions of 40,6 and 40,8 are favored). One would anticipate a reduced E_a if the reorientation of PD-Tempone is induced by the flexible motions of the hydrocarbon chains. In fact, this explanation is supported by the observation that the E_a for PD-Tempone in hydrocarbon solvents (e.g., hexane and decane) is about 3–5 kcal/mol, while for a nonmesogenic solvent with a central dipolar region and hydrocarbon end chains (e.g., di-*n*-butylphthalate) one obtains an E_a = 8.5 kcal/mol. The case for 8CB appears to show an opposite trend in the N ↔ S_A phases, although, unfortunately the range of the nematic phase is too scanty to obtain reliable results on E_a in this phase. A preliminary interpretation of this phase would be that in the nematic phase the PD-Tempone is already expelled into the hydrocarbon regions, but the expansion of the interlayer spacings with decreasing temperature somehow allows the PD-Tempone back into a region closer to -C≡N groups. Further experiments with other liquid crystals related to 8CB would be useful here.

In the cases of 40,6 and 40,8 one finds $\tau_R(C)/\tau_R(B)$ range from 1.24 to 1.42 and from 1.11 to 1.33, respectively, as T is decreased. These results may be fitted to a model of anisotropic diffusion where N_y increases gradually from 2.0 (near the N → S_A transition) to 2.8 (near the S_A → S_B transition) for 40,6 and ranging from 1.6 to 2.6 for 40,8. (The anisotropic viscosity model requires more drastic variations in $\bar{N}$ of 6 to 15 for 40,6 and 3 to 11 for 40,8 and is thus less preferred as an explanation.) The case of 8CB, in which $\tau_R(C)/\tau_R(B)$ ranges from 0.97 to 0.90 as T is decreased, is fit with a model in which N_y decreases from 1.0 to 0.4, or alternatively one can use x axis ordering to yield an N_x increasing from 1.0 to 1.6. (In this case anisotropic viscosity fails miserably even requiring *negative* values of $\bar{N}$ at the lower temperatures.) Our own preference is a SRLS model,[1,10] which allows us to translate an $N_y \sim 2$ (or an $N_x \sim 2$) into an $S_1^2\tau_x \sim {}^2/_3\tau_R$ (where S_1 is the order parameter for the SRLS and τ_x its relaxation time, cf. section 5). The increase in N_y as T decreases would thus be consistent with an increase in S_1^2, even while the mean ordering $\langle D^2_{00}\rangle_y$ experienced by the PD-Tempone is decreasing in this phase for 40,6 and 40,8. This is not at all unreasonable in the context of our model in which the flexible end chains are interpenetrating more, and their dynamical motions interfere with their average, but not necessarily their instantaneous, ordering.

(4) *Smectic B Phase.* The ordering tensor for the S_A → S_B transition was characterized by only a small change in $\langle D^2_{00}\rangle_y$, but a significant change in $\langle D^2_{20} + D^2_{-20}\rangle_y$ which goes from near zero (but positive) values in S_A to substantial negative values in S_B. This amounts to a substantial increase in $|\langle D^2_{00}\rangle_x|$ and decrease in $|\langle D^2_{00}\rangle_z|$ (both of which are negative), cf. Table IV. Thus, the freezing-in of the smectic layered structure, which characterizes the S_B phase, appears to require the PD-Tempone to relocate itself in a new region, or more likely (see below) there is some partial constraining of the hydrocarbon end chains, so the fluctuations in ordering in the molecular x–z plane (or more rigorously the smectic x''–y'' plane), which we have suggested tend to average out in the S_A phase, no longer do so in the S_B phase. [In the case of the N → S_A transition, the ordering tensor increases, but the relative changes of the components are, at least to a rough approximation, of the same order (cf. Table IV).]

The changes in spin relaxation in crossing the S_A → S_B transition are even more dramatic. First, there is a significant *decrease* in both $\tau_R(B)$ and $\tau_R(C)$ in passing into the S_B phase, although the E_a values do not appear to be altered significantly for 40,8 (the result for 40,6 in the S_A phase is rather uncertain), and secondly the $\tau_R(C)/\tau_R(B)$ ratio increases from 1.3 to 1.8 in 40,6 and from 1.33 to 2.15 in 40,8. This is further evidence of the changed character of the local environment of PD-Tempone that occurs at this phase transition.

TABLE IV: Typical Order Parameters for PD-Tempone in Liquid Crystal Solvents

	T = 74.3 °C N	T = 52.4 °C S_A	T = 35 °C S_B
	40,6		
$\langle D^2_{00}\rangle_x$	−0.006	−0.037	−0.087
$\langle D^2_{00}\rangle_y$	+0.047	+0.107	+0.107
$\langle D^2_{00}\rangle_z$	−0.041	−0.070	−0.020
	T = 74.5 °C N	T = 57.7 °C S_A	T = 42.0 °C S_B
	40,8		
$\langle D^2_{00}\rangle_x$	−0.008	−0.047	−0.081
$\langle D^2_{00}\rangle_y$	+0.050	0.116	0.114
$\langle D^2_{00}\rangle_z$	−0.042	−0.069	−0.033
	T = 37.6 °C N	T = 29.8 °C S_A	
	8CB		
$\langle D^2_{00}\rangle_x$	−0.006	−0.082	
$\langle D^2_{00}\rangle_y$	0.069	0.142	
$\langle D^2_{00}\rangle_z$	−0.063	−0.060	

As the temperature decreases in the S_B phase, $\tau_R(B)$ and $\tau_R(C)$ both increase as expected, while the ratio $\tau_R(C)/\tau_R(B)$ remains nearly constant till the S_B → solid transition is reached.

These observations are somewhat reminiscent of observations made for PD-Tempone in phase V about the nematic to solid transition (as a function of pressure, cf. ref 10, Figure 6a). In this earlier study, the C/B ratio (or alternatively $\tau_R(C)/\tau_R(B)$) was found to gradually increase in the nematic phase as the N → C transition was approached, while in the (unordered) crystalline phase the C/B ratio is unusually large at the phase transition, but C/B approaches unity as one moves away from the transition and deeper into the crystalline phase. Furthermore, $\tau_R(B)$ and $\tau_R(C)$ actually *decrease* as one moves deeper into the crystalline phase. (However, $\tau_R(B)$ values on either side of the N → solid transition were found to be comparable.) These results were interpreted in terms of the probe being located in a cavity in the solid phase with a structure like that in the nematic phase, except that increasing the pressure freezes out movement of the solvent molecules, so the motion of the spin probe becomes less hindered. The large C/B ratio would then be due to a SRLS effect which is then frozen out and disappears with increased pressure.

While there are some important differences in our present observations of the S_A → S_B transition (and also, very importantly, the τ_R values are nearly two orders of magnitude shorter in the present case thus requiring some differences in detailed analysis of the ESR results), the similarities strongly suggest (1) a cavity-like arrangement for PD-Tempone in the S_B phase; and (2) the importance of the SRLS mechanism in modulating the geometry of the cavity. Thus, our present model involves a partial freezing (or slowing down) of the hydrocarbon end chains at the S_A → S_B transition such that the PD-Tempone is in a fairly well-defined cavity with reduced "frictional" restriction to its motion, so its τ_R decreases. However, the residual end-chain motions effectively modulate the structure of the cavity, and this modulation is slow enough that the SRLS mechanism makes a very appreciable

contribution to the observed line widths. This model remains essentially unchanged throughout the S_B phase. From the point of view of activation theory, the similarity in E_a for the S_A and S_B phases (e.g., 40,8) would imply a similarity in structure of the cavity in the two phases, but the difference in preexponential factors imply that the thermally induced rate of "effective collisions" causing the PD-Tempone to surmount the barrier is significantly increased in the S_B phase (and this latter somewhat surprising statement may again be likened to the enhanced rotational mobility previously observed for PD-Tempone in the solid phase of phase V as we have already discussed).

From the point of view of the fluctuating torque model[1,10,24] we may write $\tau_R = IV^2\tau_M/6kT$, where I is the moment of inertia of the PD-Tempone, V^2 the mean-square value of the fluctuating torques, while τ_M is the relaxation time associated with the fluctuating torques. One may suppose that τ_M shows the temperature behavior characterized by E_a, and the decrease in τ_R in passing from $S_A \rightarrow S_B$ phases is largely due to a reduction in V^2. This point of view more naturally summarizes our above discussion. To complete this point of view we must recognize that V^2 and τ_M are characteristic of the fairly rapid fluctuating torques which induce the reorientation such that $\tau_M < \tau_R$, while the SRLS mechanism is due to fluctuating torque components for which $\tau_X > \tau_R$ (where τ_X is the relaxation time for the SRLS process). Thus the $S_A \rightarrow S_B$ transition would be further characterized by an increase in slowly fluctuating torque modes at the expense of the more rapidly relaxing torque modes.

(5) *SRLS Mechanism from Line Widths.* We may summarize the effect of SRLS on the ESR line widths by writing modified expressions for the spectral densities $J_{0M}(\omega)$ and $J_{2M}(\theta)$. Thus we have[1,10]

$$J_{0M}(\omega) = \frac{1}{5}\frac{\tau(0)}{1+\omega^2\tau(0)^2} \rightarrow \frac{1}{5}\left[D_0(\omega) + \frac{S_l^2\tau_x}{1+\omega^2\tau_x^2}\right] \quad (7a)$$

and

$$J_{2M}(\omega) = \frac{1}{5}\frac{\tau(2)}{1+\omega^2\tau(2)^2} \rightarrow \frac{1}{5}D_2(\omega) \quad (7b)$$

where the first equality is the usual definition of the spectral density for anisotropic diffusion in an isotropic liquid,[1,8] and the arrow points to the form appropriate for SRLS. [Note that $\tau(0)^{-1} \equiv 6R_\perp + 4R_\parallel$ and $\tau(2)^{-1} \equiv 2R_\perp + 4R_\parallel$.] The best current form we have for $D_0(0)$ and $D_2(0)$ is based upon Table VII, and is

$$D_0(0) = [1 + 0.1884S_l - 2.576S_l^2 + 1.2694S_l^3]\tau(0) \quad (8a)$$

$$D_2(0) = [1 + 0.0126S_l + 0.3790S_l^2 + 0.0846S_l^3]\tau(2) \quad (8b)$$

for $0 \leq S_l \leq 0.8$, and

$$D_0(0) = [1 - 0.0940S_l - 2.4988S_l^2 - 5.2634S_l^3]\tau(0) \quad (9a)$$

$$D_2(0) = [1 - 0.0334S_l + 0.0908S_l^2 - 1.492S_l^3]\tau(2) \quad (9b)$$

for $-0.4 < S_l \leq 0$. While these numerical coefficients are not quite the same as those previously given,[10] they nevertheless yield very similar results. (One criterion for the accuracy of these numerical fits to polynomials is the fact that one can show that quite generally[25] the coefficients of the terms linear in S_l must vanish. We see in the above expressions that they are indeed small.) However, one finds that for reasonable values of $S_l^2 \lesssim 0.1$, $D_0(0) \approx \tau(0)$ and $D_2(0) \approx \tau(2)$, so we will ignore these small corrections.

The SRLS term has been generalized to the case of ordered fluids,[25] and one obtains for an axially symmetric local order parameter, S_l

$$J_{KM}(\omega) = J_{KM}^{(1)}(\omega) + J_{KM}^{(2)}(\omega) + J_{KM}^{(3)}(\omega) \quad (10)$$

where $J_{KM}^{(1)}(\omega)$ is the spectral density for overall rotational reorientation (e.g., $(1/5)(\tau_R/1 + \omega^2\tau_R^2)$ for isotropic fluids with $\tau(0) = \tau(2) = \tau_R$), which, in principle, includes the corrections analogous to those of eq 8 and 9 for the isotropic phase, while

$$J_{KM}^{(2)}(\omega) + J_{KM}^{(3)}(\omega) = \frac{1}{5}[5\kappa(0,M)]^2\delta_{K,0}\langle|S_l|^2\rangle\left[\frac{\tau_x}{1+\omega^2\tau_x^2} - \frac{\tau_R'}{1+\omega^2\tau_R'^2}\right] \quad (11)$$

where $\tau_R'^{-1} \equiv \tau_R^{-1} + \tau_x^{-1} \simeq \tau_R^{-1}$ and $\kappa(0,M)$ are given in Table VI. The generalization for nonaxially symmetric long-range as well as local ordering is given in Appendix B. One may now look at the effect of the SRLS correction. This is first done for the simpler expressions (eq 7) appropriate for isotropic liquids, when we assume $\omega_n^2\tau_x^2 << 1$ (where ω_n are the ^{14}N spin-flip frequencies) which appears reasonable in light of the very rapid τ_R values obtained in this work (cf. Figure 10), for which $\omega_n^2\tau_R^2 << 1$ is certainly true. For isotropic liquids and anisotropic rotation one has[1,10] $\tau(0)/\tau(2) = {}^1/_3(2N+1)$ with $N = R_\parallel/R_\perp$. Now suppose there is isotropic rotation (i.e., $\tau(0) = \tau(2)$) but a SRLS mechanism given by eq 7 [but ignoring any effects of S_l on $D_0(0)$ and $D_2(0)$] is present. Then there will be an "apparent" $\tau'(0) \approx \tau(0) + S_l^2\tau_x$, and therefore an "apparent" $N' \approx (3/2)[[\tau'(0)/\tau(2)] - 1/3]$. Thus we see how a satisfactory fit of the ESR relaxation data to a model of anisotropic rotational diffusion could be equally well fit by a SRLS model. One then would need independent considerations, such as those discussed above, to distinguish between them. [However, in the work of I and ref 10, where $\omega_n^2\tau_x^2 \gtrsim 1$, the line width effects of the two models become distinguishable.] One finds that for weak ordering, such as that experienced by PD-Tempone, the $\kappa(K,M)$ correction factors in eq 11 or their generalization in Appendix B are not large; they do not differ very significantly from unity. Thus the main point we have made here (viz. that the effects of SRLS lead to an "apparent" $N' \neq 1$) is essentially unchanged. Further K-dependent relaxation from SRLS can result from the effects of a nonaxial local ordering of the probe (cf. Appendix B).

It is suggested in Appendix B that $\tau_x = \tau_x(M)$, and this can further modify the "apparent" effects of SRLS, e.g., the M dependence would lead to the same type of line width effects as an anisotropic viscosity model (i.e., $\hat{N} \neq 1$). Another M-dependent model discussed in Appendix B is for a local tilted director, where the projection of the tilt in the lab x–y plane fluctuates in time.

These, then, are the considerations which allow us to discuss our line width results either in terms of anisotropic rotation or viscosity or else in terms of the SRLS mechanism. Combination models are discussed in Appendicies B and C.

Last of all, we note that we have not introduced any consideration of jump types of models. We show in Appendix D that this is not important for the weakly ordered PD-Tempone probe.

(D) *Angular Dependence of the Line Widths.* In this work, as is typical in magnetic resonance studies, the magnetic field was employed to align the director in the sample. In the nematic phases, because the director follows the dc magnetic field (~3 kG), it is impossible to study the angular dependence of the line width unless other

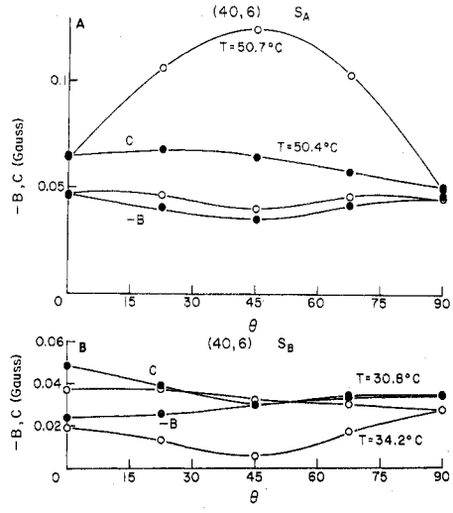

Figure 12. Angular dependence of B and C in (40,6) when the director is tilted by angle θ with respect to the magnetic field. The open circles are the experimental data taken with 2-mm i.d. cylindrical tube; closed circles are taken with 0.5-mm i.d. tube: (A) smectic A phase, (B) smectic B phase.

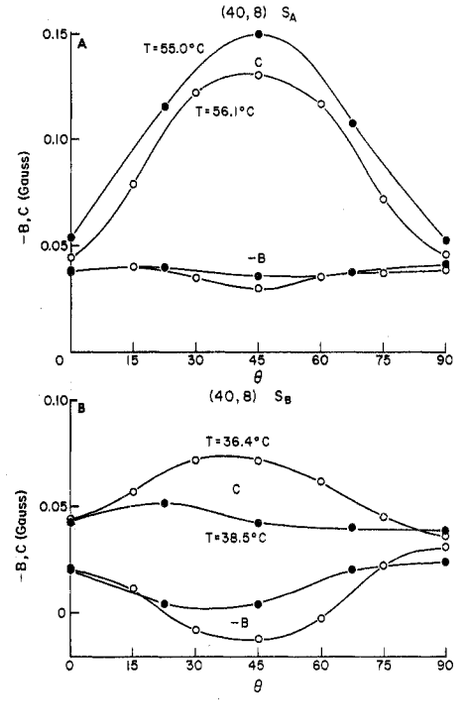

Figure 13. Angular dependence of B and C in (40,8). The open circles are taken with 2-mm i.d. cylindrical tube and the closed circles are taken with 0.5-mm i.d. tube: (A) smectic A phase; (B) smectic B phase.

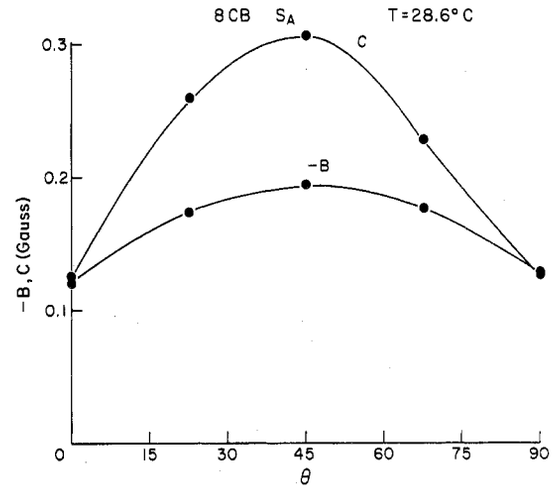

Figure 14. Angular dependence of B and C in 8CB smectic A phase. The experimental data are taken in 0.5-mm i.d. tube.

external constraints are introduced (e.g., electrical fields and/or very thin glass plates[26]). We have studied the angular dependences for the smectic A and smectic B phases. The results already discussed showed that, with the exception of 8CB in the larger 2 mm i.d. tubes, the S_A and S_B phases had their alignments "locked-in" so the director could be tilted relative to the magnetic field without reorienting. The orientational dependence of the g shifts and hyperfine shifts are in complete agreement with what is predicted for the "locked-in" director (cf. Figure 4). The angular dependences of the line widths in the smectic A and smectic B phases were first analyzed in the same manner as in the different phases for 0° tilt. We first simulated the ESR spectra at various orientations to obtain the appropriate (angular dependent) $\langle a_D \rangle$ for correcting the line widths due to deuteron inhomogeneous broadening (cf. Figure 3). This lead to the surprising result that the angular dependences of the $\langle a_D \rangle$ appear to be different for the two different tube diameters. Just as surprising was the observation that the angular dependences of C and B (as well as C/B) were very much dependent upon the tube diameter even though the results for 0° tilt (as well as 90° tilt) were found to be virtually independent of tube size. Typical angular variations of B and C are shown in Figures 12–14. We discuss aspects of these results below.

First of all, we wish to examine the importance of having accurate $\langle a_D \rangle$ values in order to obtain the correct values of line width parameters A, B, and C for the PD-Tempone probe. Based upon our initial uncertainty of the correct angular dependence of $\langle a_D \rangle$, we considered the implications of using different values of $\langle a_D \rangle$. In this way, one rapidly becomes convinced that significant changes in the $\langle a_D \rangle$ used will (1) have virtually no effect on the C/B ratio; (2) have only a marginal effect on the values of C and B; (3) have an appreciable effect on the values of A. Thus, for example, a dramatic 40% increase in postulated $\langle a_D \rangle$ (from −0.0222 to −0.0309) is found to decrease A by 25%, while B and C are only decreased by 4.5% and the C/B ratio only varies by 0.5%, for lines with intrinsic width ca. 0.2 G. A less dramatic increase of $\langle a_D \rangle$ of 14% yielded respective decreases in A, B, C, and C/B of 6.5, 1.4, 1.1, and −0.2%. We thus concluded that our results for C/B as well as B and C could be regarded as reliable even when there was some uncertainty in the correct values of $\langle a_D \rangle$ required. The angular-dependent results for $\langle a_D \rangle$ given in Table I for 40,6 are the most reliable ones we obtained. The reasons for this are discussed below. The angular dependence of the $\langle a_D \rangle$ is expected to follow the relation $\langle a_D \rangle = [a_D + {}^1/_2(3\cos^2\theta - 1)\chi_D]$ (see Appendix A). One finds from Table I that for $\langle a_D \rangle$ this is approximately, but not exactly, obeyed unlike the results for $\langle a_N \rangle$, which were in exact agreement.

It is our belief that these anomalous observations may be explained in terms of inhomogeneous broadening due to a static distribution of the directors in the smectic phases which results from the effects of (i) the strength, geometry, and smoothness of the anchoring of the smectic layering by the tube walls, (ii) the elastic constants determining the strength of the smectic ordering in the bulk of the phase, and (iii) the effects of the magnetic-field induced torques (due to the diamagnetic anisotropy of the samples), which try to reorient a tilted director into an alignment parallel to the magnetic field. Thus, in the extreme case of 8CB, the anchoring forces as transmitted

TABLE V: Line Shape Asymmetries for 40,6, 40,8, and 8CB in Different Phases[a]

phase	low field ($M = +1$)	center ($M = 0$)	high field ($M = -1$)
	A. 40, 6		
isotropic	1.00(0.971)	0.980(0.979)	0.960(0.961)
nematic	1.01(0.979)	0.980(0.957)	0.970(0.960)
S_A 0°	1.023(0.939)	0.985(0.864)	0.964(0.888)
22.5	1.020(0.962)	0.988(0.881)	0.985(0.904)
45	1.018(0.859)	0.991(0.906)	0.968(1.045)
67.5	0.990(0.854)	0.981(0.927)	0.996(1.056)
90°	0.980(0.926)	0.992(0.943)	1.024(0.979)
S_B 0°	0.996(0.934)	0.994(0.921)	1.000(0.943)
22.5°	0.999(0.918)	0.998(0.914)	1.001(0.933)
45°	1.001(0.895)	0.994(0.911)	0.988(0.928)
67.5°	1.006(0.925)	1.003(0.938)	0.993(0.949)
90°	0.997(0.940)	1.002(0.949)	0.999(0.961)
	B. 40,8		
isotropic	0.989(1.031)	0.985(0.990)	0.983(0.963)
nematic	1.010(0.981)	0.958(0.997)	0.943(0.963)
S_A 0°	1.18(0.99)	0.97(0.96)	0.80(0.92)
22.5°	1.02(1.14)	0.97(0.99)	0.85(0.87)
45°	1.00(1.14)	0.97(1.03)	0.95(0.94)
67.5°	0.89(1.01)	0.99(0.96)	1.10(1.03)
90°	0.87(0.99)	0.98(0.92)	1.11(1.00)
S_B 0°	1.10(1.002)	1.061(0.948)	0.868(0.973)
22.5°	0.936(1.07)	1.064(0.965)	0.891(0.940)
45°	1.026(1.06)	0.934(0.983)	0.994(0.935)
67.5°	0.886(1.01)	0.909(0.994)	1.052(0.980)
90°	0.884(0.953)	0.907(1.003)	1.057(1.001)
	C. 8CB		
isotropic	0.994(0.985)	0.989(0.986)	0.986(0.985)
nematic	1.034(1.001)	0.966(0.974)	0.945(0.966)
S_A 0°	1.12(1.007)	0.911(0.983)	0.861(0.963)
22.5°	1.12(1.007)	0.892(0.983)	0.876(0.963)
45°	1.02(1.007)	0.963(0.983)	0.900(0.963)
67.5°	0.908(1.007)	1.050(0.983)	1.109(0.963)
90°	0.912(1.007)	1.048(0.983)	1.059(0.963)

[a] Table entries are for R = (low field max amplitude)/(high field max amplitude) in a derivative ESR spectrum. Numbers first given are for 0.5-mm i.d. tubes; those in parentheses are for 2.0-mm i.d. tube. Precision ranges from ±0.001 to ±0.01.

by the aligning forces (elastic constants) of the smectic phase are too weak to maintain a fixed alignment for 2-mm diameter tubes, but not for 0.5-mm tubes, as the sample is tilted relative to the magnetic field. Nevertheless, even when the samples appear to be well aligned by virtue of the correct variation of a_N with tilt (and by simple optical methods), there is a small static distribution of directors.

The presence of this source of small inhomogeneity superimposed upon the small inhomogeneity due to $\langle a_D \rangle$ is undoubtedly the reason for an apparent variation of $\langle a_D \rangle$ with sample size. Since it appeared difficult to deconvolute these two sources of small inhomogeneity from each other, we chose a rather simple criterion for distinguishing the effects of static director distributions. The composite lines observed in the absence of such effects are very nearly anti-symmetric about their centers (cf. Figure 3). However, we found that the composite lines, where such effects were believed to be present, were asymmetric. We therefore used such an asymmetry as a measure of these effects, i.e., one lets R be the ratio of the low-field to high-field extremum amplitude of a hyperfine line. Then an $R \neq 1$ is a definite indication of inhomogeneous broadening. Our results for R are summarized in Table V. We find that only in the case of 40,6 in the 0.5-mm tubes, are the values of R in the S_A and S_B phases in the range of 0.98–1.02, which we regard as antisymmetric within experimental error. [Also, in 8CB in 2-mm tubes, where the magnetic field completely re-aligns the director, very good line shape symmetry is observed independent of the sample angle.] We thus regard our angular-dependent results for $\langle a_D \rangle$, A, B, C, and C/B for 40,6 in 0.5-mm tubes as our most reliable, which if not entirely devoid of effects of static director fluctuations, then they are at least small. On the other hand, our results for 40,8 show worse asymmetries for 0.5-mm tubes than for 2-mm tubes. We suspect that some intermediate size tube would be optimum for this solvent. Significant asymmetries are observed for 8CB in 0.5-mm tubes.

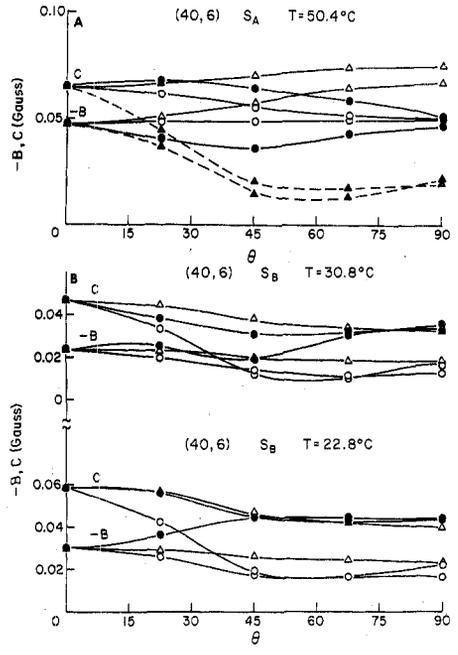

Figure 15. (A) Angular dependence of B and C in (40,6) smectic A phase. Closed circles are experimental data taken with 0.5-mm i.d. tube. Open circles are the theoretical fits with $N = \hat{N} = 2.34$ and $\tau_{R\perp} = 1.28 \times 10^{-11}$ s. △ is the theoretical fit with $N = 2.81$, $\hat{N} = 1$, and $\tau_{R\perp} = 1.51 \times 10^{-1}$ s. ▲ is the fit with $N = 1$, $\hat{N} = 11.5$, and $\tau_{R\perp} = 6.57 \times 10^{-11}$ s. (B) Angular dependence of B and C in (40,6) S_B phase. Closed circles are experimental data taken with 0.5-mm tube. For $T = 30.8$ °C, the theoretical fit with $N = \hat{N} = 8.2$ and $\tau_{R\perp} = 6.09 \times 10^{-11}$ s is represented by O; and the fit with $N = 51.8$, $\hat{N} = 1$, $\tau_{R\perp} = 8.15 \times 10^{-11}$ s is represented by △. For $T = 22.8$ °C, the theoretical fit with $N = \hat{N} = 7.0$, $\tau_{R\perp} = 7.62 \times 10^{-11}$ s is represented by O, and the fit with $N = 39.3$, $\hat{N} = 1$, $\tau_{R\perp} = 1.01 \times 10^{-10}$ s is represented by △.

Our further objectives will be to (1) analyze the most reliable results (viz. 40,6 solvent and 0.5-mm diameter tube) in terms of spin relaxation (section E) and (2) to examine further aspects of the problem of static distributions of directors in the smectic phases (section F).

(E) *Angular Dependence of the Spin Relaxation.* We have seen in the previous section that the angular-dependent line widths in the smectic phases typically include both inhomogeneous broadening associated with these phases as well as the homogeneous widths due to spin relaxation. However, in the case of 40,6 in 0.5-mm tubes, we were able to sufficiently remove the former, that we could attempt an analysis of the latter in terms of spin relaxation. Our analysis of angular-dependent relaxation is again based upon equations given in I.[27,28] We first attempted to employ in our analysis of the angular-dependent results, the fits at $\theta = 0°$ found using the models of anisotropic rotation and of anisotropic viscosity. These are shown in Figure 15. In the case of S_A, neither the model with $N = 2.81$, $\hat{N} = 1$ nor the model with $N = 1$, $\hat{N} = 11.5$ showed satisfactory agreement with the angular dependent results (although they agree with the $\theta = 0°$ results).

Now, in principle, there is no reason not to consider models with combined anisotropic rotation and viscosity.[29] However, there is a fundamental theoretical problem in developing such a model. This results from the fact that the principal axis systems for the two types of anisotropy (the molecular and lab frames respectively) are rapidly fluctuating with respect to one another. Therefore, the diffusion tensor $\mathbf{R}(t)$ defined in any coordinate frame will, in general, still be time dependent. This problem is discussed at some length in Appendix C, where general forms of the diffusion operator are considered which yield time-independent relaxation eigenvalues even when $\mathbf{R}(t)$ is still time dependent in any one frame.

We show in Figure 15 predictions using a particular form, which minimizes adjustable parameters, and may be written simply when we momentarily neglect the effects of ordering as

$$\tilde{\Gamma}_\Omega \boldsymbol{D}^L_{KM}(\Omega) = R_\perp[L(L+1) + (N-1)K^2 + (\hat{N}-1)M^2]\boldsymbol{D}^L_{KM}(\Omega) \quad (12)$$

This is subject to the restriction that $N \geq 1$ and $\hat{N} \geq 1$ (cf. Appendix C). We first fixed $N = \hat{N}$ and then found the optimum set of values for $R_\perp$ and N which fit the $\theta = 0°$ results. These values were then used to predict the experimental results for $\theta \neq 0°$ as shown in Figure 15. We see in Figure 15A that this exhibits considerably improved agreement with experiment, even yielding exact agreement at $\theta = 90°$ within experimental error. (Recall that the $\theta = 0°$ and $\theta = 90°$ experimental results for B and C are quite insensitive to effects of inhomogeneous broadening associated with sample tube size and shape.) We have varied the ratio $N/\hat{N}$ between the two limiting cases (i.e., $N = 1$ or $\hat{N} = 1$), but we find the best agreement for $N = \hat{N}$. Also, we have tested a simple case based on a model in Appendix C such that $L(L+1)$ in eq 12 is changed to $2L(L+1)$ (cf. eq C7) and $N \approx \hat{N}$. This case could not even yield agreement with the $\theta = 0°$ results for any values of the adjustable parameters.

Similar analyses were made for the S_B phase as shown in part in Figure 15B. In this case the model based upon eq 12 and $N = \hat{N} \approx 7$ to 8 showed an improved shape of angular dependence for B vs. C compared to the original results for $N \approx 40$ to 50 and $\hat{N} = 1$, but the predictions for $\theta = 90°$ are displaced from the experimental results. Variations of the models, as discussed for the S_A case, did not improve the fits.

As we discussed for the results at $\theta = 0°$, we believe the angular-dependent effects are most likely due to a SRLS mechanism rather than actual anisotropic rotation or diffusion. We note from the general discussion of Appendix B, that one can generate dependences of the $J^{SRLS}_{K,M}(\omega)$ on both K and M, so that, following the lines given in section C5, one could go about fitting the angular dependence to these models with considerable leeway in the adjustable parameters ($\tau_x(M)$ and S_{1K}).

Clearly, we have not exhaustively studied all possible combination models. Nor do our present experimental results necessarily warrant them. However, we are encouraged by the improved agreement to believe that angular-dependent relaxation studies can provide a basis for studying such phenomena. Clearly, one requires (1) accurate forms of the orienting potential; (2) adequate knowledge of the orientation dependence of any unresolved proton or deuteron splittings, and (3) adequate knowledge of any effects of static distribution of directors due to distortions in the smectic phases.

F. *Static Distribution of Directors.* We now consider in further detail static distributions of directors and their effect on the line width and line shape as a function of tilt angle θ of the mean director with respect to the magnetic field. We may for this case write as the derivative line shape function (cf. I)

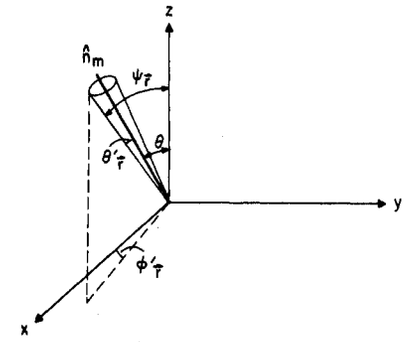

Figure 16. Coordinate system representing a sample rotated by angle θ in the laboratory frame so that $\hat{n}_m$ lies in the lab x–z plane. There is a static distribution of local directors with polar and azimuthal angles $\theta'_{\vec{r}}$ and $\varphi'_{\vec{r}}$ relative to $\hat{n}_m$. The local director makes an angle of $\psi_{\vec{r}}$ with the lab z axis.

$$I(B_0,\theta,\vec{r}) = \int_0^\pi \sin\theta_{\vec{r}}'\, d\theta_{\vec{r}}' \times \int_0^{2\pi} d\varphi_{\vec{r}}' \frac{T_2^{-1}(\Psi(\vec{r}))[B(\Psi(\vec{r})) - B_0]}{[T_2^{-1}(\Psi(\vec{r}))]^2 + [B(\Psi(\vec{r})) - B_0]^2} P_{eq}(\Psi(\vec{r})) \equiv \int_0^\pi \sin\theta_{\vec{r}}'\, d\theta_{\vec{r}}' \int_0^{2\pi} d\varphi_{\vec{r}}' I(B_0,\Psi(\vec{r}))\, P_{eq}(\Psi(\vec{r})) \quad (13)$$

where $\Psi(\vec{r}) = (0,\psi_{\vec{r}},\varphi_{\vec{r}}')$ are the Euler angles for a particular director $\hat{n}(\vec{r})$ relative to the lab frame as shown in Figure 16. The lab frame is defined by the magnetic field along the z axis and the mean director $\hat{n}_m$ in the x–z plane. The particular $\hat{n}(\vec{r})$ is tilted from $\hat{n}_m$ by polar and aximuthal angles $\theta_{\vec{r}}'$ and $\varphi_{\vec{r}}'$, respectively, and

$$\cos\psi_{\vec{r}} = \cos\theta\cos\theta_{\vec{r}}' - \sin\theta\sin\theta_{\vec{r}}'\cos\varphi_{\vec{r}}'$$

$B(\Psi(\vec{r}))$ is the resonant field for spin probes at $\vec{r}$. It is given by eq A12 and A13 where $\boldsymbol{D}^2_{00}(0,\theta,0)$ is replaced by

$$\boldsymbol{D}^2_{00}(0,\psi_{\vec{r}},\varphi_{\vec{r}}') = \sum_N \boldsymbol{D}^2_{0N}(0,\theta_{\vec{r}}',\varphi_{\vec{r}}')\boldsymbol{D}^2_{N\,0}(0,\theta,0) = \frac{4\pi}{5}\sum_N (-)^N Y_{2N}(\theta_{\vec{r}}',\phi_{\vec{r}}')Y_{2N}(\theta,0) = \boldsymbol{D}^2_{00}(0,\psi_{\vec{r}},0) \quad (14)$$

Also $P_{eq}(\Psi(\vec{r}))$ is the distribution function for the angles $\theta_{\vec{r}}',\varphi_{\vec{r}}'$. A simple form used by others[1,5,6a,30-33] is $P_{eq}(\Psi) \propto e^{-\alpha\sin^2\theta'}$ independent of $\vec{r}$, but the φ' dependence has usually been ignored, although this is not strictly correct for $\theta \neq 0$. We wish to consider more appropriate forms for this distribution function, in particular, the effects of the magnetic interaction between the magnetic field and the diamagnetic susceptibility of the mesophase.

The interaction energies which are most important in the smectic phase include[34,35] (1) the smectic layering free energy, represented by $^1/_2\bar{B}(\partial u/\partial z')^2$ where $\bar{B}$ is the elastic constant for compression of the layers and $u(\vec{r})$ measures the displacement of the smectic layer from equilibrium at point $\vec{r}$; (2) the free energy of splay distortion: $^1/_2K_1 \cdot [(\partial^2 u/\partial x'^2) + (\partial^2 u/\partial y'^2)]^2$, where K_1 is the associated elastic constant; the magnetic free energy: $-^1/_2\chi_a(\hat{n}(\vec{r})\cdot\vec{B})^2 = -^1/_2\chi_a B_0\cos^2\psi_{\vec{r}}$, where χ_a is the anisotropy in the diamagnetic susceptibility. Thus we have

$$F_{sm} = {}^1/_2\bar{B}\left(\frac{\partial u}{\partial z'}\right)^2 + {}^1/_2K_1\left(\frac{\partial^2 u}{\partial x'^2} + \frac{\partial^2 u}{\partial y'^2}\right) - {}^1/_2\chi_a B_0\cos^2\psi_{\vec{r}} \quad (15)$$

for the smectic free energy per unit volume in the bulk of the phase. If we now identify $\hat{n}_m$ with the normal to the smectic layers at equilibrium, then $\hat{n}(\vec{r})$ representing a particular director at $\vec{r}$, would be characterized by the distortions $n_{x'} = -\partial u/\partial x' \ll 1$ and $n_{y'} = -\partial u/\partial y' \ll 1$.

Another important consideration is that of the boundary effects or wall alignment.[35] It is known that glass walls typically tend to align the smectic layers parallel to the wall. (When this alignment is strong one speaks of "strong anchoring".) This alignment cannot be satisfactorily achieved in cylindrical capillary tubes. (In fact one may anticipate in such cases an alignment where the smectic layers form in concentric cylinders about the tube axis. This is known as a myelinic texture.) Thus, the alignment procedure that is typically used, which involves cycling from the nematic to smectic A phases in the presence of very large magnetic fields, relies on the magnetic free energy to favor the alignment of the smectic layers to be perpendicular (for positive diamagnetic anisotropy) to the field. Samples prepared in this way may still experience distortions at the wall surfaces which are not perpendicular to the magnetic field (as well as distortions due to wall imperfections). Unfortunately, little is known about the strength of these boundary effects, so one usually only considers the effects of strong anchoring.[34,35] We shall outline an approximate discussion of distortions leading to a static distribution of directors on this basis, and use it to discuss our experimental situation.

One starts by integrating eq 15 over all $\vec{r}$ and then Fourier analyzing by letting[34,35,38]

$$u(\vec{r}) = \sum_{\vec{q}}^{q_c} u(\vec{q}) e^{i\vec{q}\cdot\vec{r}} \tag{16}$$

(where q_c is the cutoff wave vector, where $q_c \sim \pi/b$ with b a molecular dimension) so that

$$n_{x'}(\vec{q}) = iq_{x'}u(\vec{q}) \tag{17a}$$

$$n_{y'}(\vec{q}) = -iq_{y'}u(\vec{q}) \tag{17b}$$

Note that the fact that $u(\vec{r})$ is real requires that $u(-\vec{q}) = u^*(\vec{q})$ in eq 16. Thus we obtain

$$F_{vol} = \sum_{\vec{q}}^{q_c} \frac{V}{2} [\bar{B}q_{z'}^2 + K_1 q_\perp^4 + \chi_a B_0^2 (q_{x'}^2 \cos 2\theta + q_{y'}^2 \cos^2\theta)]|u(\vec{q})|^2 \tag{18}$$

Here $q_\perp^2 = q_{x'}^2 + q_{y'}^2$. In order to obtain this simple result for the contribution of the magnetic free energy, we have dropped terms linear and cubic in the $u(\vec{q})$. The linear term does disappear upon integrating over $\vec{r}$ [i.e., one uses $1/V\int e^{i\vec{q}\cdot\vec{r}}\,d\vec{r} \propto \delta(\vec{q})$], while the cubic terms are dropped on the assumption that the $u(\vec{q})$'s are small enough that terms higher order than quadratic are not needed. Strong-anchoring boundary effects will limit the values of $\vec{q}$ allowed in the expansion of eq 18. It follows from eq 18 and equipartition that the mean square values of $u(\vec{q})$ are given by

$$\langle|u(\vec{q})|^2\rangle = \frac{k_B T/V}{\bar{B}q_{z'}^2 + k_1 q_\perp^4 + \chi_a B_0^2 [q_{x'}^2 \cos 2\theta + q_{y'}^2 \cos^2\theta]} \tag{19}$$

and then we have

$$\langle|n_+(\vec{q})|^2\rangle = q_\perp^2\langle|u(\vec{q})|^2\rangle = (k_B T)/\left[(q_{z'}^2/q_\perp^2) + \lambda^2 q_\perp^2 + \lambda^2 \xi_B^{-2} \left(\cos 2\theta \frac{q_{x'}^2}{q_\perp^2} + \cos^2\theta \frac{q_{y'}^2}{q_\perp^2} \right) \right] \bar{B}V \tag{20}$$

where $n_+(\vec{q}) = n_x(\vec{q}) + in_y(\vec{q})$. Here we have introduced the parameters $\lambda \equiv (K_1/\bar{B})^{1/2} \sim a$ the layer thickness and $\xi_B \equiv (K_1/\chi_a B_0^2)^{1/2}$ the coherence length due to the presence of the magnetic field. For typical values[34] of $K_1 \sim 10^{-6}$ dyn, $\chi_a \sim 10^{-7}$, $B_0 \sim 10^4$ G and $\lambda \sim 2 \times 10^{-7}$ cm (corresponding to $\bar{B} = 2.5 \times 10^7$ dyn/cm^2), one has $\lambda^2\xi_B^{-2} \sim 4 \times 10^{-7}$. We can now estimate $\langle|n_+(\vec{r})|^2\rangle \simeq V/(2\pi)^3 \cdot \int_0^{q_c} d\vec{q}\langle|n_+(\vec{q})|^2\rangle$. We have performed this integration numerically using eq 20, and the values given above (as well as $q_c \sim \pi \times 10^7$ cm^{-1}) to obtain in the absence of a magnetic field:

$$\langle|n_+(\vec{r})|^2\rangle \approx \frac{k_B T}{K_1 \pi^2} \times 8.88 \times 10^{-7}$$

(with a slightly greater than linear dependence upon q_c). We may compare this result with the equivalent result for a nematic in the one constant approximation (for which[34,35] $\langle|n_+(\vec{q})|^2\rangle = 2k_B T/[K_1 V(q^2 + \xi_B^{-2})]$) to obtain

$$\langle|n_+(\vec{r})|^2\rangle \approx \frac{k_B T}{K_1 \pi^2} q_c \approx \frac{k_B T}{K_1 \pi^2} \times 3.14 \times 10^7 \approx 0.33$$

(Because these results depend strongly upon a somewhat arbitrary choice of cutoff q_c, they should only be considered in terms of rough order of magnitude estimates.) Thus we see that while $\hat{n}(\vec{r})$ experiences substantial fluctuations for the nematic phase, these fluctuations are greatly suppressed by the forces in the smectic phase which maintain the layer structure [from the term $^1/_2\bar{B}(\partial U/\partial z')$]. It is thus unlikely that in a magnetic resonance experiment, wherein one obtains the signal integrated over the whole sample, that one can anticipate any measurable effects from such weak fluctuations. Furthermore, these fluctuations are dynamic viscous modes,[34,35] and their relaxation must further reduce their contribution to line widths in a magnetic resonance experiment.[25] In fact, neither in this work nor in previous work (cf. I) have we observed any effects from the much more substantial fluctuations in the nematic phase on PD-tempone line widths.

In the case of light scattering experiments, one normally does not observe even those fluctuations which require very little energy in a smectic (i.e., the pure undulation modes for which $q_{z'} \to 0$ so that the smectic energy term $\bar{B}q_{z'}^2 \to 0$). Instead, one observes the effects of static distortions which are transmitted deep into the bulk (from wall distortions and/or localized defects) by the very same smectic aligning forces.[34,36] Thus, for a wall undulation of wavelength $2\pi/q_{x'}$, the thickness L of the distorted region [i.e., the decay constant for $u(\vec{r})$] is given by $L = 1/q_{x'}^2\lambda$ which is much larger than the result $L = 2\pi/q_{x'}$ for a nematic. We could therefore expect to see ESR line shape distortions from such effects in the smectic phase, when they are unobservable in the nematic. Now $u(\vec{r})$ resulting from such effects could also be Fourier analyzed (cf. eq 16) [away from the sources: either the wall or localized defects], and one could then expect some statistical distribution for the $\langle|u(\vec{q})|^2\rangle$ as well as the $\langle|n_+(\vec{q})|^2\rangle$.

We now wish to consider possible effects of the magnetic field, as the angle θ is varied. For the simpler case of parallel-plate smectic alignment with strong anchoring, any distortion $u(\vec{r})$ that is induced vanishes for both $z' = 0$ and d (where d is the sample thickness), so we may restrict any modes $u(\vec{q})$ induced to $q_{z'} = n\pi/d$ with $n = 1, 2, 3$ and with $n = 1$ corresponding to the easiest mode to distort, since the $\bar{B}(\partial u/\partial z)^2$ term is smallest. Now normally such distortions (1) are expected to require very high fields (ca. 60 kG) and (2) are expected to be of such low amplitude as to be unobservable even by light scattering.[34,35] These are again due to the effects of the smectic aligning forces

(e.g., $\chi_a B_c^2 = 2\pi(\bar{B}K_1/d)^{1/2}$ with B_c being the critical field). However, for our samples the anchoring is not very strong. Thus, we may expect to have modes $q_{z'} = \pi/d'$, where $d' > d$ is an "effective" sample thickness, and also the restraining forces for such distortion modes are weaker because of the weaker anchoring. In those cases in which the anchoring is sufficiently weak (e.g., 8CB in 2-mm tubes) there is total realignment of the smectic phases by the magnetic field, but for somewhat stronger anchoring (e.g., 40,6 and 40,8) distortions about the mean director may well be expected. These effects should enhance the $\langle|n_+(\vec{r})|^2\rangle$ that will be observed.

We now return to a consideration of the above effects on eq 13. First the ESR signal involves integrating $I(B_0,\theta,\vec{r})$ over the whole sample. We then let

$$\bar{I}(B_0,\theta) \equiv \int d\vec{r}\, I(B_0,\theta,\vec{r}) \tag{21}$$

If the distortion modes are small enough, then $I(B,\Psi(\vec{r}))$ (cf. eq 13) may be expanded in a Taylor's series about the equilibrium orientation $\hat{n}_m$. That is

$$I(B,\Psi(\vec{r})) = [I(B,\Psi(\vec{r}))]_{n_+(\vec{r})=0} + \left[\frac{\partial I(B,\Psi(\vec{r}))}{\partial n_+(\vec{r})}\right]_{n_+(\vec{r})=0} [n_+(\vec{r})] + \left[\frac{\partial^2 I(B,\Psi(\vec{r}))}{\partial^2 n_+(\vec{r})}\right]_{n_+(\vec{r})=0}\left[\frac{n_+(\vec{r})}{2}\right]^2 + \text{H.O.T.} \tag{22}$$

and $I(B_0,\theta)$ obtained by integration over $\theta_{\vec{r}}'$, $\varphi_{\vec{r}}'$ with $P_{eq}(\Psi(\vec{r}))$. Now the nature of wall anchoring and other wall effects, etc. guarantees that $P_{eq}(\Psi(\vec{r}))$ will be a function of $\vec{r}$, which is best handled by Fourier analysis. Thus, if we know from statistical and other[34-36] considerations the distribution function for the $\vec{q}_i$th mode, $P_{eq}(\theta_{\vec{q}_i}',\varphi_{\vec{q}_i}')$ we may make use of the complete $P_{eq}(\Psi(\vec{q}))$ [defined in a manner similar to Appendix A of ref 25 for all values of $\vec{q}$ as a product of the individual $P_{eq}(\Psi(\vec{q}_i))$] in order to obtain the absorption signal given by eq 21 which is averaged over the sample

$$\bar{I}(B_0,\theta) = V[I(B_0,\Psi(\vec{r}))]_{n_+(\vec{r})=0} + \tfrac{1}{2}\sum_{\vec{q}_i}^{q_c}\langle n_+(\vec{q}_1)n_+(-\vec{q}_1)\rangle \times \left[\frac{\partial^2 I(B_0\Psi(\vec{r}))}{\partial n_+(\vec{r})^2}\right]_{n_+(\vec{r})=0} + \text{H.O.T.} \tag{23}$$

where the angular brackets again imply averaging over θ' and φ'.

The question arises as to the importance of the higher order terms (H.O.T.) in the expansion even for small fluctuations. In particular [with $I(B_0,\psi(\vec{r}))$ given by eq 13 the derivative of a Lorentzian] the term $\partial^m I(B_0,\Psi(\vec{r})/n_+(\vec{r})^m$ may be shown to involve the $(m+1)$th derivative of the Lorentzian line shape. For a very sharp line these higher derivatives would tend to cause the Taylor's series expansion to diverge (i.e., in the limit $T_2 \to \infty$ the Lorentzian approaches a Dirac delta function whose derivatives are increasingly more singular). Thus, it is not sufficient to require that $n_+(\vec{r})$ be small in order to achieve rapid convergence of the series. Another criterion for convergence should therefore be that the quantity $T_2^2[B(\Psi(\vec{r})) - \bar{B}]^2$, where $\bar{B}$ is the resonant field in the absence of ordering (e.g., in the isotropic phase), be small. Unfortunately, we have found that for PD-Tempone in the liquid crystals studied here, the ESR widths are so sharp that the Taylor's series shows no sign of convergence even after terms through fourth order are included when values are used which can lead to observable effects on the ESR spectra (e.g., increased ESR line widths as a function of tilt angle θ). (Such expansions were compared to the full integrations for the simple examples given below showing no agreement.) This perhaps emphasizes the considerable sensitivity of the narrow line shapes obtained in this work to such static fluctuations.

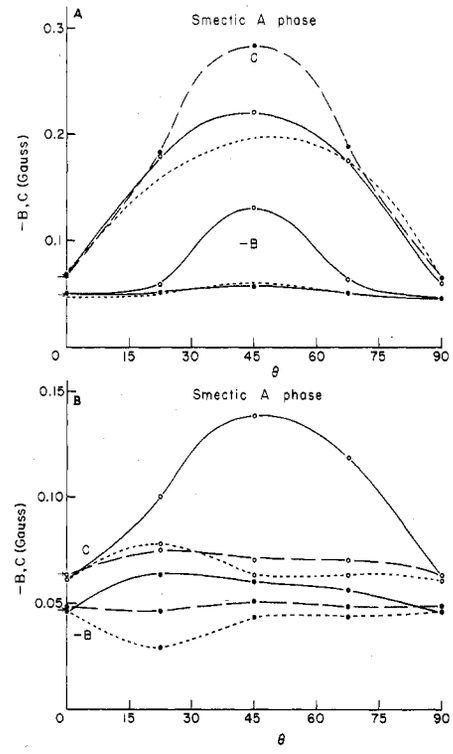

Figure 17. The angular dependence of B and C for PD-Tempone calculated from a static distribution of directors and a magnetic-field pulling effect for order parameters appropriate for the S_A phases: (A) $\alpha_0 = 500$ and (—) $\alpha_1 = 0$, (----) $\alpha_1 = 2.5$, (····) $\alpha_1 = 10$, (B) $\alpha_1 = 2.5$ and (—) $\alpha_0 = 650$, (----) $\alpha_0 = 800$, (····) $\alpha_0 = 1000$. The input homogeneous values of B and C (assumed angular independent) are shown as arrows on the ordinate.

As a result of this problem, we found it necessary to perform the full integrations over $\theta_{\vec{r}}'$ and $\varphi_{\vec{r}}'$. The simplest approach is to assume that we can replace the sum over $\vec{q}$ modes such as those which appear in eq 23 and instead we approximate eq 21 by

$$I(B_0,\theta) \approx \int_0^{\pi} \sin\theta'\, d\theta' \int_0^{2\pi} d\varphi'\, I(B_0,\Psi)\, P_{eq}(\Psi) \tag{24}$$

where $P_{eq}(\Psi)$ is a simple distribution function in Ψ that implicitly includes any $\vec{r}$ dependence. For our calculations we assumed $P_{eq}(\Psi)$ in the absence of magnetic-field effects would show a "one-sided" Gaussian distribution about θ', while the effect of the magnetic field would, as suggested by eq 15, be represented by a term in $\cos^2\psi$. That is we let

$$P_{eq}(\Psi) \approx Ne^{(-\alpha_0\sin^2\theta'+\alpha_1\cos^2\psi)} \tag{25}$$

and considered various values of α_0 and α_1.

We show some of our results in Figure 17 for the S_A phase and Figure 18 for the S_B phase. In general, the dependence upon α_0 and α_1 is complex, but a comparison of Figure 17 with Figure 12A for (40,6) shows that the predictions are in reasonable agreement with experiment. We would estimate for the 2-mm i.d. tube in this case an $\alpha_0 \sim 600$ and an $\alpha_1 \sim 5$–10, while in the 0.5-mm capillary tube $\alpha_0 \sim 900$ and $\alpha_1 \sim 2.5$. In general, the asymmetries of the lines for the range of parameters shown are determined by the ratio α_1/α_0: the asymmetries are greater for larger values of this ratio, while almost no asymmetry

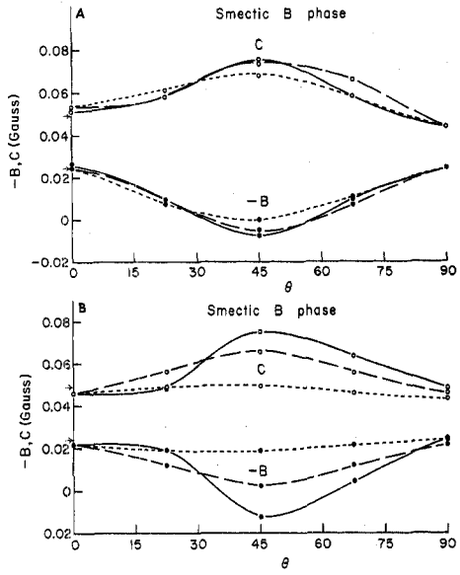

Figure 18. The angular dependence of B and C for PD-Tempone calculated from a static distribution of directors and a magnetic-field pulling effect for order parameters appropriate for the S_B phases: (A) $\alpha_0 = 500$ and (—) $\alpha_1 = 0$, (----) $\alpha_1 = 5.0$, (····) $\alpha_1 = 10$; (B) $\alpha_1 = 2.5$ and (–) $\alpha_0 = 400$, (----) $\alpha_0 = 600$, (····) $\alpha_0 = 800$. The input homogeneous values of B and C (assumed angular independent) are shown as arrows on the ordinate.

is predicted as $\alpha_1/\alpha_0 \rightarrow 0$; (e.g., for $\alpha_0 = 500$, $\alpha_1 = 0$, and $\theta = 45°$ one has for the +1, 0, and –1 lines: $R = 0.98$, 1.00, and 0.98, respectively; while for α_1 changed to 2.5, it becomes 0.90, 1.00, and 1.08; and for α_1 changed to 10 it becomes 0.73, 1.00, and 1.26). These asymmetries bear a reasonable, but not a precise, relation to the results in Table VI, (the largest discrepancy being that little or no asymmetry is predicted for $\theta = 0°$, although this is not necessarily the case for the experimental results). We would estimate for (40,8) (cf. Figure 13a) in the 2-mm. i.d. tube, values similar to those for (40,6), while for the 0.5-mm tube a small decrease in these values. It appears that for 8CB in the 0.5-mm tube (cf. Figure 14), $\alpha_0 \sim 400$–500 while $\alpha_1 \sim 1$ or 2, which is a little surprising.

One might attempt to improve the model calculations by superposing the results for different sets of α_1 and α_0 (to crudely simulate different modes). This will undoubtedly have a further effect on both the predicted widths and the asymmetries, since there are small shifts of the resonance centers, primarily for the outer two lines (and are typically a little smaller than the difference in inhomogeneous broadening predicted for the two modes). However, we felt this additional effort was not at present justified.

Similar comments apply for the comparisons of Figures 12B and 13B with typical predictions for the S_B phases shown in Figure 18. Note, in particular, the rather good agreement of the results for (40,8) in 2-mm i.d. tubes with the predictions in Figure 18A.

We do wish to note that the values predicted for B and C at 0° tilt are quite insensitive to the model parameters α_1 and α_0, and they do lie close to the input values. This is also true to a lesser extent for 90° tilt. This prediction is in agreement with our observations.

One may wonder about the effect on these calculations of any uncertainty in the determination of the ordering tensor. Actually, such uncertainties will have virtually no effect. This may be seen from eq A12, A13, and A14. Equations A12 and A13 show that $\langle a \rangle$ and $\langle g \rangle$ are just the observed hyperfine and g shifts (except for a very small high-field correction in eq A13. It is only necessary to use these experimental values (or more precisely the curve drawn through them) in Figures 4, or alternatively the $\langle \boldsymbol{D}^2_{00} \rangle$ and $\langle \boldsymbol{D}^2_{20} + \boldsymbol{D}^2_{20} \rangle$ which are directly related to them by either eq A14 or 3. Also, we have found that the inhomogeneous broadening that is predicted increases approximately linearly with the magnitude of the order parameters.

In summary we note the fact that for (40,6) it appears possible to suppress distortions by going to a smaller diameter sample (i.e., by decreasing d) is consistent with the suppression of any distortions due to (1) defects which may exist in the bulk and (2) defects from a tilted magnetic field. However the fact that for (40,8) the smaller diameter samples lead to *changes* in the inhomogeneous line shape characteristics (cf. Table V) is more consistent with wall distortions being transmitted to the bulk. The case of 8CB showing that, for the large tubes, the bulk solution follows the magnetic-field alignment, and the line shapes do not appear to have inhomogeneous contributions, strongly suggests the importance of magnetic-field enhanced distortions in those samples in which the smectic alignment remains otherwise fixed as the sample is reoriented in the magnetic field. These phenomena are complex and are perhaps better studied in samples with simpler anchoring geometries (e.g., parallel-plate alignment),[37] although we do note the reproducibility and the excellent "mean alignment" (manifested by $\langle a_N \rangle$ and $\langle g \rangle$) that can be obtained by cycling with strong magnetic fields.

IV. Summary and Conclusions

We have shown in this work how the methods previously employed by Polnaszek and Freed in I to study spin relaxation in nematic liquid crystals using the weakly ordered PD-Tempone spin probe may be employed in a study of smectic phases. The observations of ordering and spin relaxation in the isotropic and nematic phases of the liquid crystals studied here (40,6, 40,8, and 8CB) were very similar to the previous results and were analyzed similarly. This includes (1) the use of a two-term orienting potential for the PD-Tempone; (2) the observation of comparable activation energies for reorientation (E_a) (except for 8CB) which are characteristic of those associated with the solvent viscosity; (3) the similarity of the relaxation behavior in these two phases.

In the smectic phases significant differences are observed. The isotropic hyperfine interactions are found to have decreased from their value in the isotropic phase. This was attributed to a (partial) expulsion of the PD-Tempone from the dipolar region of the liquid-crystalline molecules (which is preferred by the polar PD-Tempone molecule) toward the more flexible hydrocarbon end chains as a result of the packing of the smectic layers. The analysis of the hyperfine interactions was based on empirical fits of a_N and a_D to solvent polarity. This model is further supported by the fact that the E_a for the reorientation process are found to decrease substantially in the smectic phases to values characteristic of hydrocarbon solvents. Furthermore, there is a significant change in the nature of the rotational reorientation, that could be interpreted in terms of increased rotational anisotropy (which is exceedingly large for the smectic B phase). However we believe it is physically more reasonable to interpret our observations in terms of a slowly-relaxing local structure (SRLS) model due to the slow fluctuations of the hydrocarbon chains. In passing from $S_A \rightarrow S_B$ phases one finds significant changes in (1) the hyperfine interaction which decreases further, (2) the ordering tensor, which becomes significantly more nonaxial, (3) the rate of reorientation, which increases significantly, and (4) the spin

relaxation anomaly we attribute to SRLS which also increases significantly. All these observations are consistent with a model in which the smectic B phase is more solidlike with the more rigid layer-packing causing the PD-Tempone to be expelled further out to the hydrocarbon end chains, and into more well-defined "cavities" experiencing more slowly-relaxing fluctuations of the end chains.

Differences in results observed for 40,6 and 40,8 on the one hand and 8CB on the other [viz. (1) decreasing ordering with decreasing temperature for the former, but the opposite for the latter and (2) an apparently small E_a in the nematic and a larger E_a in the smectic for 8CB] is rationalized in terms of differences in the nature of the smectic A phase for these two types of liquid crystals. Thus, the 40,6 and 40,8 have interlamellar spacings that are a little smaller than the molecular length and this spacing decreases with decreasing temperature, while 8CB has a bilayer lamellar structure with an interlamellar spacing that expands with decreasing temperature. Thus, in the latter case the PD-Tempone probes may be able to move closer to the polar C≡N end groups as the temperature is reduced.

An observation we have made that is of some significance for studies of spin relaxation in smectics (in particular studies of the variation of line widths with orientation of the magnetic field), is the fact that the orientation-dependent line widths show a significant dependence on the size and shape of the sample even when the hyperfine and g shifts show that the sample remains well-aligned even as it is rotated (or tilted) relative to the magnetic field. This dependence on sample size was not of any significance for 0° tilt angle, and this appears to be reasonably the case for a tilt of 90°. However, it becomes very significant for intermediate values of the tilt angle. This phenomenon is discussed in terms of inhomogeneous broadening due to static distortions of the smectic layering and to distortions of the director, which tries to remain perpendicular to the smectic layering. Such distortions may result from wall anchoring effects and/or dislocations in the bulk, as well as from torques on the smectic alignment due to a tilted magnetic field. In the smectic phase the large free-energy associated with the layering results in persistence of such distortions over much greater lengths in the sample than for nematic phases. While the effects of magnetic torques are expected to be small for well-anchored smectics, the typical magnetic resonance technique of alignment in a tube by recycling into the phase in the presence of a strong magnetic field undoubtedly leads to not very strong anchoring, as evidenced by the failure of 8CB to maintain its alignment in larger (2-mm i.d.) tubes. Only in the case of 40,6 was it possible to suppress such effects by using smaller (0.5-mm i.d.) tubes. Our simple model calculations of these effects are in semiquantitative agreement with most of the observations. In our theoretical discussion of these matters we also considered the effects of fluctuations of the director in the smectic phase, but concluded that they were much too weak to be of importance, since they are much weaker than for nematics, and no observable effects from fluctuations within the nematic phase are seen with PD-Tempone probe.

We have discussed the angular-dependent line widths for 40,6 in 0.5-mm i.d. tubes in terms of combined models of anisotropic rotation and anisotropic viscosity. The theoretical problem of how to analyze such a model, when the two relevant axis systems are rapidly fluctuating with respect to each other, so the rotational-diffusion tensor is time dependent in any reference frame, is discussed in an

TABLE VI: Mean Square Values of the Rotation-Matrix Elements $D^L_{KM}(\Omega)$ Including Cross Terms for Nonaxially Symmetric Ordering[a]

$\kappa(K,K',M)$[b,c]			
K	K'	M	function of ordering tensor
0	0	0	$\frac{1}{5}+\frac{2}{7}\langle D^2_{00}\rangle_\Omega+\frac{18}{35}\langle D^2_{00}\rangle_\Omega-\langle D^2_{00}\rangle_\Omega{}^2$
0	0	1	$\frac{1}{5}+\frac{1}{7}\langle D^2_{00}\rangle_\Omega-\frac{12}{35}\langle D^4_{00}\rangle_\Omega$
0	0	2	$\frac{1}{5}-\frac{2}{7}\langle D^2_{00}\rangle_\Omega+\frac{3}{35}\langle D^4_{00}\rangle_\Omega$
2	2	0	$\kappa(0,0,2)-\lvert\langle D^2_{20}\rangle_\Omega\rvert^2$
2	2	1	$\frac{1}{5}-\frac{1}{7}\langle D^2_{00}\rangle_\Omega-\frac{2}{35}\langle D^4_{00}\rangle_\Omega$
2	2	2	$\frac{1}{5}+\frac{2}{7}\langle D^2_{00}\rangle_\Omega+\frac{1}{70}\langle D^4_{00}\rangle_\Omega$
2	0	0	$-(\frac{2}{7}+\langle D^2_{00}\rangle_\Omega)\langle D^2_{20}\rangle_\Omega+(9/7\sqrt{15})\langle D^4_{20}\rangle_\Omega$
2	0	1	$-\langle D^2_{20}\rangle_\Omega/7-6\langle D^4_{20}\rangle_\Omega/(7\sqrt{15})$
2	0	2	$2\langle D^2_{20}\rangle_\Omega/7$
2	−2	0	$6\langle D^4_{40}\rangle_\Omega/\sqrt{70}$
2	−2	1	$-\langle D^4_{40}\rangle_\Omega/\sqrt{70}$
2	−2	2	$\langle D^4_{40}\rangle_\Omega/\sqrt{70}$

[a] From ref 29. [b] $\kappa(K,K',M)$ defined by eq B2. [c] Other values may be obtained from eq B5.

TABLE VII: Zero-Frequency Spectral Densities $J^{(i)}_{KM}(0)$ for the Isotropic Brownian Reorientation of a Molecule Experiencing a Reorienting Potential $U(\beta)/kT=-\lambda\cos^2\beta^{a-c}$

K	M	a_0	a_1	a_2	a_3
			$S>0$ to 0.8		
0	0	1.000	3.008	−9.704	5.654
0	1	1.000	1.084	−2.769	0.397
0	2	1.000	−2.117	1.181	−0.097
1	2	1.000	−1.058	−0.307	0.288
2	2	1.000	2.148	0.664	−0.028
1	1	1.000	0.567	9.425	4.854
			$S<0$ to −0.4		
0	0	1.000	2.010	−5.972	−12.243
0	1	1.000	0.983	−3.741	−2.254
0	2	1.000	−2.223	0.480	−4.783
1	2	1.000	−1.088	−0.410	−0.004
2	2	1.000	2.116	0.397	−1.338
1	1	1.000	0.357	8.004	−7.472

[a] The table lists $5J^{(i)}_{KM}(0)/\tau_R=(a_0+a_1S+a_2S^2+a_3S^3)$ with $S=\langle D^2_{00}(0,\beta,0)\rangle_\Omega$. [b] These results were calculated by Dr. C. F. Polnaszek. [c] See Table II of ref 25 for further details.

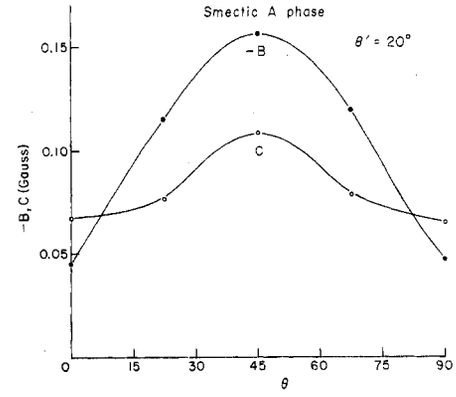

Figure 19. The angular dependence of B and C calculated for the model of the S_A phase in which the director is tilted with respect to $\hat{n}_m$ by 20°, but the projection in the x'–y' plane is randomly oriented.

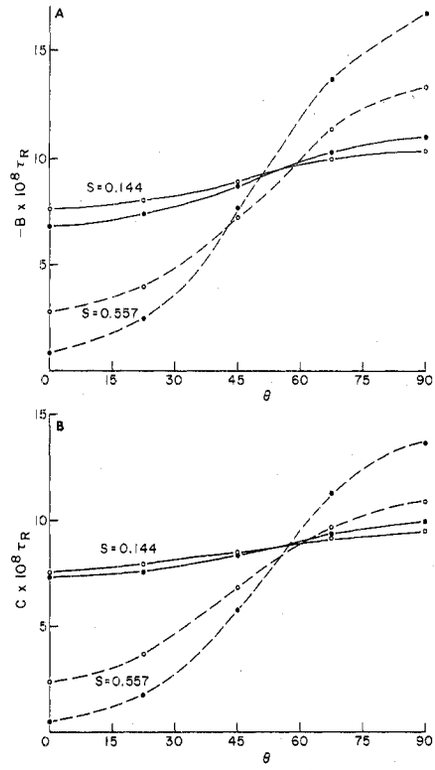

Figure 20. Predictions of the comparison of the angular-dependence of (A) B and (B) C for Brownian motion and strong jump models of reorientation. The solid lines indicate results for weak ordering (e.g., PD-Tempone) with $\langle D^2_{00} \rangle = 0.144$, while the dashed lines are for strong ordering with $\langle D^2_{00} \rangle = 0.557$ (e.g., CSL). The solid circles are for Brownian motion, while the open circles are for strong jump.

Appendix. Improved agreement with experiment is obtained for the S_A phase from such a model. Analogues of such combined models for the case of SRLS are also developed in an Appendix. Again we favor the SRLS mechanisms for the present physical situations. It is our belief that studies of angular-dependent spin relaxation will, in the future, prove useful in enabling one to elucidate the details of complex dynamical processes. However, it is clear that it will be important to deal unambiguously with effects of inhomogeneous broadening in samples, anchored well enough, that they appear to have their smectic layering "locked-in" when they are tilted with respect to the magnetic field.

Acknowledgment. We thank Drs. E. Meirovitch, C. F. Polnaszek, K.V.S. Rao, and Mr. S. Zager for helpful discussions and advice and Mr. G. Barkley for his help with some of the computations.

Appendix A. Dependence of the ESR Spectrum on Angle of Tilt θ

Following I we write the perturbing Hamiltonian as

$$\mathcal{H}_1(\Omega,\Psi) = \sum_{\substack{L,K,M,M' \\ \mu,i}} (-1)^K \boldsymbol{D}^L_{-KM}(\Omega)\boldsymbol{D}^L_{M'M}(\Psi)F'_{\mu,i}{}^{(L,K)}A_{\mu,i}{}^{(L,M)} \quad \text{(A1)}$$

where the $F'_{\mu,i}{}^{(L,K)}$ and $A_{\mu,i}{}^{(L,M)}$ are the irreducible tensor components of rank L, with F' in molecule-fixed coordinates, while A is a spin operator quantized in the laboratory axes (whose z axis coincides with the applied dc field). Equation A.1 is based upon two sets of rotations of the coordinate systems. This may be seen by writing the A' in molecule-fixed coordinates as

$$A'_{\mu,i}{}^{(L,-K)} = \sum \boldsymbol{D}^L_{-KM}(\Omega)\boldsymbol{D}^L_{M'M}(\Psi)A_{\mu,i}{}^{(L,M)} \quad \text{(A1a)}$$

Thus the first rotation is from the laboratory axis system (x,y,z) into the director axis system (x'',y'',z'') with Euler angles Ψ which may be specified by polar angles θ,φ such that $\Psi = (0,\theta,\varphi)$, and then into the molecular axis system (x',y',z') with Euler angles $\Omega = (\alpha,\beta,\gamma)$. Since, in general, the principal axis system of the magnetic interactions (x''',y''',z''') is not identical with that for the ordering (or diffusion) of the molecule in the mesophase (x',y',z'), one may transform from the former to the latter according to

$$F'_{\mu,i}{}^{(L,K)} = \sum_{K'} \boldsymbol{D}^L_{KK'}(\Theta)F'''_{\mu,i}{}^{(L,K')} \quad \text{(A2)}$$

where $\Theta = (\alpha',\beta',\gamma')$. [Note we often drop the triple superscripts and refer to the (x''',y''',z''') as (x,y,z) when it is not easily confused with the lab frame.] In the motional narrowing region in the mesophase one has a non-zero average value of $\mathcal{H}_1(\Omega)$ specified by $\langle \mathcal{H}_1(\Omega) \rangle$, where the averaging implied by the angular brackets is according to the prescription of eq 4a. Thus we have

$$\langle \mathcal{H}_1(\Omega) \rangle = \sum_{L,K,M,M',\mu,i} (-1)^K \langle \boldsymbol{D}^L_{-KM}(\Omega) \rangle \boldsymbol{D}^L_{M'M}(\Psi)F'_{\mu,i}{}^{(L,K)}A_{\mu,i}{}^{(L,M)} \quad \text{(A3)}$$

In the case of a uniaxial director one has

$$\langle \boldsymbol{D}^L_{-KM}(\Omega) \rangle = \langle \boldsymbol{D}^L_{-K0}(\Omega) \rangle \delta_{M',0} \quad \text{(A4)}$$

The positions of the resonance lines are then determined by

$$\mathcal{H}_0' \equiv \mathcal{H}_0 + \langle \mathcal{H}_1(\Omega) \rangle \quad \text{(A5)}$$

where $\mathcal{H}_0$ is the usual zero-order Hamiltonian for isotropic liquids. Thus in the case of a single nucleus (e.g., N^{14}) one has

$$\mathcal{H}_0 = g_e\beta_e B_0 S_z + a_N S_z I_z \quad \text{(A6a)}$$

and

$$\langle \mathcal{H}_1(\Omega) \rangle = \sum_{L,K,M,\mu} (-1)^K \langle \boldsymbol{D}^L_{-K0}(\Omega) \rangle \boldsymbol{D}^L_{0M}(\Psi)F'_{\mu}{}^{(L,K)}A_{\mu}{}^{(L,M)} \quad \text{(A6b)}$$

The solution of this Hamiltonian is formally identical with that for a single crystal Hamiltonian with axially symmetric magnetic parameters,[3] i.e.

$$\tilde{F}_{\mu}{}^{(L,0)} \equiv \sum_K (-1)^K \langle \boldsymbol{D}^L_{-K0}(\Omega) \rangle F'_{\mu}{}^{(L,K)} \quad \text{(A7)}$$

Thus

$$\tilde{a}_{\parallel} = a_N + (2/3)^{1/2} \sum_K (-1)^K 2\pi\xi_N D_N{}^{(K)} \langle \boldsymbol{D}^2_{-K0}(\Omega) \rangle \quad \text{(A8a)}$$

$$\tilde{a}_{\perp} = a_N - (1/6)^{1/2} \sum_K (-1)^K 2\pi\xi_N D_N{}^{(K)} \langle \boldsymbol{D}^2_{-K0}(\Omega) \rangle \quad \text{(A8b)}$$

where $\xi_N D_N{}^{(K)}$ are the irreducible components of the hyperfine tensor (in MHz), and

$$\tilde{g}_{\parallel} = g_s + (2/3)^{1/2} \sum_K (-1)^K g^{(K)} \langle \boldsymbol{D}^2_{-K0}(\Omega) \rangle \quad \text{(A9a)}$$

$$\tilde{g}_{\perp} = g_s - (1/6)^{1/2} \sum_K (-1)^K g^{(K)} \langle \boldsymbol{D}^2_{-K0}(\Omega) \rangle \quad \text{(A9b)}$$

with $g^{(K)}$ the irreducible components of the **g** tensor. One then defines

$$g(\theta) \equiv (\tilde{g}_{\parallel}{}^2 \cos^2\theta + \tilde{g}_{\perp}{}^2 \sin^2\theta)^{1/2} \quad \text{(A10a)}$$

$$a(\theta) \equiv (\tilde{g}_{\parallel}{}^2\tilde{a}_{\parallel}{}^2 \cos^2\theta + \tilde{g}_{\perp}{}^2\tilde{a}_{\perp}{}^2 \sin^2\theta)^{1/2}/g(\theta) \quad \text{(A10b)}$$

and the resonant field is given by

$$B(\theta) = \frac{g_s}{g}B_0 - \frac{g_s}{g}aM_N - \frac{g_s^2}{g^2}\frac{(\tilde{a}_\parallel^2 + a^2)\tilde{a}_\perp^2}{4a^2B_0}[I_N(I_N+1) - M_N^2] - \frac{g_s^2}{g^2}M_N^2\left[\frac{(a_\parallel^2 - a_\perp^2)^2}{8a^2B_0}\right]\left(\frac{\tilde{g}_\parallel\tilde{g}_\perp}{g^2}\right)^2 \sin^2 2\theta \quad \text{(A11)}$$

For g values which deviate only slightly from g_s one can write

$$a(\theta) \simeq (\tilde{a}_\parallel^2 \cos^2\theta + \tilde{a}_\perp^2 \sin^2\theta)^{1/2} \quad \text{(A10c)}$$

For PD-Tempone in which the ordering is weak eq A11 may be simplified to

$$a(\theta) \simeq a_N + \boldsymbol{D}^2_{00}(0,\theta,0)(2/3)^{1/2}\sum_K(-1)^K 2\pi\xi_N D_N^{(K)}\langle \boldsymbol{D}^2_{-K0}(\Omega)\rangle \equiv \langle a\rangle \quad \text{(A12a)}$$

$$g(\theta) \simeq g_s + \boldsymbol{D}^2_{00}(0,\theta,0)(2/3)^{1/2}\sum_K(-1)^K g^{(K)}\langle \boldsymbol{D}^2_{-K0}(\Omega)\rangle \equiv \langle g\rangle \quad \text{(A12b)}$$

where $\boldsymbol{D}^2_{00}(0,\theta,0) = (1/2)(3\cos^2\theta - 1)$, and

$$B(\theta) \simeq B_0\left(2 - \frac{\langle g\rangle}{g_s}\right) - M_N\langle a\rangle - \frac{a_N^2}{2B_0}[I(I+1) - M_N^2]\left[1 - \left(\frac{\langle a\rangle}{a_N} - 1\right) - 2\left(\frac{\langle g\rangle}{g_s} - 1\right)\right] \quad \text{(A13)}$$

where we have only kept terms to lowest power in $\langle \boldsymbol{D}^2_{K0}(\Omega)\rangle$. Equation A13 is the form used in eq 13.

When one only has non-zero $\langle \boldsymbol{D}^2_{00}(\Omega)\rangle_{z'}$ and $\langle \boldsymbol{D}^2_{20}(\Omega) + \boldsymbol{D}^2_{-20}(\Omega)\rangle_{z'}$ and parallel molecular (x,y,z) and (x',y',z') axes, then we have

$$\langle a\rangle - a_N = \left[(a_{z'} - a_N)\langle \boldsymbol{D}^2_{00}\rangle_{z'} - \frac{1}{\sqrt{6}}(a_{x'} - a_{y'}) \times \langle \boldsymbol{D}^2_{20} + \boldsymbol{D}^2_{-20}\rangle_{z'}\right]\boldsymbol{D}^2_{00}(0,\theta,0) \quad \text{(A14a)}$$

and

$$\langle g\rangle - g_s = \left[(g_{z'} - g_s)\langle \boldsymbol{D}^2_{00}\rangle_{z'} - \frac{1}{\sqrt{6}}(g_{x'} - g_{y'}) \times \langle \boldsymbol{D}^2_{20} + \boldsymbol{D}^2_{-20}\rangle_{z'}\right]\boldsymbol{D}^2_{00}(0,\theta,0) \quad \text{(A14b)}$$

In the case of y ordering which is used in this paper one makes the appropriate substitutions of the axes (i.e., $y = z'$, $z = x'$, $x = y'$). Equations A14 lead to eq 3 used to determine the order parameters from the hyperfine line shifts.

One may also use an analogous set of formulae to deal with the unresolved deuteron (or proton) super-hyperfine structure. However, the magnetic principal axis system for each deuteron is not generally coincident with the (x',y',z') system (even after averaging over rapid methyl group motions). Also, the deuterons (or protons) have anisotropic hyperfine tensors that are much larger than the isotropic hyperfine splittings, so even though the ordering in (the analogue) of eq A8a is small, these anisotropic terms make a large contribution. Thus one should use the analogue of eq A10c in place of eq A12a, with analogues of eq A8 for $\tilde{a}_{\parallel,D}$ and $\tilde{a}_{\perp,D}$. One finds that for the two-term ordering, eq A8 become

$$\tilde{a}_{\parallel,D} = a_D + \chi_D \quad \text{(A15a)}$$

$$\tilde{a}_{\perp,D} = a_D - \tfrac{1}{2}\chi_D \quad \text{(A15b)}$$

with

$$\chi_D = (a_{z'z',D} - a_D)\langle \boldsymbol{D}^2_{00}\rangle_{z'} - \frac{1}{\sqrt{6}}(a_{x'x',D} - a_{y'y',D})\langle \boldsymbol{D}^2_{2,0} + \boldsymbol{D}^2_{-2,0}\rangle_{z'} \quad \text{(A16)}$$

That is, the other non-zero components of the hyperfine tensor in the (x',y',z') axes are averaged out. It would appear therefore that by measurements of χ_D in different phases exhibiting different values of $\langle \boldsymbol{D}^2_{00}\rangle_{z'}$ and $\langle \boldsymbol{D}^2_{2,0} + \boldsymbol{D}^2_{-2,0}\rangle_{z'}$, (e.g. the S_A and S_B phases) the values of $a_{z'z',D} - a_D$) and $a_{x'x',D} - a_{y'y',D}$) could be found. (However contributions from small, but nonvanishing ordering components such as $\langle \boldsymbol{D}^2_{2,0} - \boldsymbol{D}^2_{-2,0}\rangle_{z'}$ would affect χ_D, while such components are not detected from studying $\langle a_N\rangle$, because of the (near) coincidence of the (x''',y''',z''') magnetic axes and the (x',y',z') ordering axes.)

Appendix B. Generalizations of the SRLS Mechanism

We consider the SRLS mechanism from the theoretical point of view recently presented by Freed.[25] The results given there were for axially-symmetric ordering, but they may be readily generalized to nonaxial molecular ordering to give the following result:

$$J^{SRLS}_{K-K',M}(\omega) = 5[\sum_{K''}\kappa(K,K''M)][\sum_{K''}\kappa(K',K'',M)] \times \left[\frac{\tau_x}{1+\omega^2\tau_x^2} - \frac{\tau_R'}{1+\omega^2\tau_R'^2}\right]\langle S_{1,K''}{}^* S_{1K}\rangle \quad \text{(B1)}$$

where $\tau_R'^{-1} \equiv \tau_R^{-1} + \tau_x^{-1} \simeq \tau_R^{-1}$ since we require $\tau_R^{-1} >> \tau_x^{-1}$. Also

$$\kappa(K,K''M) = \int d\Omega\, P_{eq}(\Omega)(\boldsymbol{D}^{2*}_{KM}(\Omega) \times \boldsymbol{D}^2_{K''M}(\Omega) - \langle \boldsymbol{D}^2_{KM}(\Omega)\rangle_\Omega\langle \boldsymbol{D}^{2*}_{K''M}(\Omega)\rangle_\Omega) \quad \text{(B2)}$$

with $P_{eq}(\Omega)$ given by eq 4b and τ_x is the SRLS relaxation time. Equation B1 is based upon the assumption that the SRLS is characterized by uniaxial primary ordering and a local structure whose fluctuations may be averaged uniformly over orientational space; i.e., one first writes as the irreducible tensor components of the local ordering

$$S_{1,K,M} = S_{1K}\boldsymbol{D}^2_{0,M}(\Psi) \quad \text{(B3)}$$

where $S_{1,K}$ is the Kth irreducible tensor component of the local order parameter (assumed small in the theory), and then we let

$$\langle S^*_{1,K'M'}(\Psi_0)S_{1,K,M}(\Psi)\rangle = \langle S^*_{1K'}S_{1K}\rangle e^{-t/\tau_x}\delta_{M,M'} \quad \text{(B4)}$$

where $\langle S^*_{1K'}S_{1K}\rangle$ are averaged over the fluctuations in S_{1K}. In general, the $\tau_x = \tau_x(M)$, and this functional dependence may be inserted into eq B1. (Also, τ_x^{-1}, may in general, include a translational component due to the diffusion of the probe from one local structure environment to another. In the latter case one might also properly include some variation of $\mathbf{R}$ in the different local regions.) One can show that for the potential of eq 5 the $\kappa(K,K',M)$ obey the symmetry relations[29]

$$\kappa(K,K',M) = \kappa(-K,-K',M) = \kappa(K,K',-M) = \kappa(-K,-K',-M) = \kappa(K',K,M) \quad \text{(B5)}$$

Also K and K' must both be either even or odd for non-zero values of $\kappa(K,K',M)$. We present in Table VI a listing of the values of $\kappa(K,K',M)$ that are needed when the two-term ordering tensor based upon eq 5 applies. Note that in this

case it should be sufficient to specify the local ordering by non-zero values of just $S_{1,0}$ and $S_{1,2} = S_{1,-2}$ which are real quantities, so the K and K' values in eq B1 need only include these values. In the case where the primary molecular ordering is axially symmetric, although the local ordering is not, then eq B1 simplifies to

$$J^{\mathrm{SRLS}}_{-K-K',M}(\omega) = 5\kappa(K,M)\kappa(K',M)\left[\frac{\tau_x}{1+\omega^2\tau_x{}^2} - \frac{\tau_{\mathrm{R}}{}'}{1+\omega^2\tau_{\mathrm{R}}{}'^2}\right]\langle S^*_{1K'}S_{1K}\rangle \quad \text{(B6)}$$

where $\kappa(K,M) \equiv \kappa(K,K,M)$.

A model has been proposed for the S_A phase which can explain the facts that (1) typically the interlayer spacing is less than the molecular length and (2) $S_A \rightarrow S_C$ transitions often occur. It is based on the idea that the molecules in the S_A phase are actually tilted by angles θ' and φ' relative to the normal to the smectic layering, but, unlike the S_C phase, there is no long-range order in φ'.[18] If we assume that the angle φ' is randomly fluctuating at each local site, then we have a SRLS model, which we can represent following Freed.[25] One lets the (dimensionless) orienting potential (in which we assume axial symmetry for simplicity) be given by the sum of two terms

$$y(\Omega) = \bar{\lambda}_0{}'\boldsymbol{D}^2_{00}(\Omega) + \bar{\lambda}_1\boldsymbol{D}^2_{00}(\Omega - \Psi) \quad \text{(B7)}$$

where $\Psi = (0,\theta',\varphi')$.

Now since

$$\boldsymbol{D}^2_{00}(\Omega - \Psi) = \sum_{N\neq 0}(-)^N\boldsymbol{D}^2_{0N}(\Omega)\boldsymbol{D}^2_{-N0}(\Psi) \quad \text{(B8)}$$

we can rewrite $y(\Omega)$ as

$$y(\Omega) = \bar{\lambda}_0\boldsymbol{D}^2_{00}(\Omega) + \bar{\lambda}_1\sum_{N\neq 0}(-)^N\boldsymbol{D}^2_{0N}(\Omega)\boldsymbol{D}^2_{-N0}(\Psi) \quad \text{(B9)}$$

where $\bar{\lambda}_0 \equiv \bar{\lambda}_0{}' + \bar{\lambda}_1\boldsymbol{D}^2_{00}(\Psi)$ is now the effective time-independent orienting potential coefficient. Now we can let

$$\boldsymbol{D}^2_{0,-N}(0,\theta',\varphi') = d^2_{0,-N}(\theta')e^{-iN\varphi'} \quad \text{(B10)}$$

where only $\varphi' = \varphi'(t)$ is time dependent. Then, by the methods given by Freed,[25] we obtain

$$J^{\mathrm{SRLS}}_{-K,M}(\omega) = (1/5)[\kappa(0,M)]^2[d^2_{0M}(\theta')]^2\delta_{K,0} \times \left[\frac{\tau_x}{1+\omega^2\tau_x{}^2} - \frac{\tau_{\mathrm{R}'}}{1+\omega^2\tau_{R'}{}^2}\right]\langle|S^2_1|\rangle \qquad M \neq 0 \quad \text{(B11)}$$

where $\kappa(0,M)$ is determined with respect to $\bar{\lambda}_0$. This result can be generalized, as before, to cases of nonaxial symmetry. Note that $[d^2_{0,0}(\theta')]^2 = (1/4)(3\cos^2\theta' - 1)^2$; $[d^2_{0,\pm1}(\theta')]^2 = (3/2)\sin^2\theta'\cos^2\theta'$; and $[d^2_{0,\pm2}(\theta')]^2 = (3/8)\cdot\sin^4\theta'$, and, in general, $\tau_x = \tau_x(M)$. Note that this mechanism would give line broadening that is formally similar to anisotropic viscosity [i.e., to eigenvalues $\hat{R}_\perp L(L+1) + M^2(\hat{R}_\parallel - \hat{R}_\perp)$ in the isotropic phase] when $\hat{R}_\parallel > \hat{R}_\perp$.

One can also calculate the predictions for such a model in the static limit, i.e., $\tau_x \rightarrow \infty$. The additional broadening for a tilt angle $\theta' = 20°$ (which is of the order to "explain" the x-ray results on interlayer thickness) calculated from a static model (i.e., eq 13 with $P_{eq}(\Psi(\vec{r}))$ a delta function in $\theta' = 20°$ and a random distribution in φ') is shown in Figure 19. This result shows extremely large contributions to $-B$, in sharp contradiction to the experimental results. Thus such a static model is inconsistent with our experiments. There is no strong reason at present to exclude the *dynamic* model discussed above.

Appendix C. The Rotational Diffusion Equation in the Presence of Both Anisotropic Rotation and Anisotropic Viscosity

In dealing with the theory of rotational reorientation in ordered liquids we have made use of the Brownian diffusion operator, which we write in symmetrized form as (cf. I)

$$\tilde{\Gamma}_\Omega = \boldsymbol{M}\cdot\mathbf{R}(t)\cdot\boldsymbol{M} + [\boldsymbol{M}\cdot\mathbf{R}(t)\cdot(\boldsymbol{M}U)]/2kT + \mathbf{T}\cdot\mathbf{R}(t)\cdot\mathbf{T}/(2kT)^2 \quad \text{(C1)}$$

where $\boldsymbol{M}$ is the operator for infinitesimal rotations and $\mathbf{R}(t)$ is the diffusion tensor of the molecule, and both are written in the (x',y',z') molecular coordinate system. The external torque $\mathbf{T}$ experienced by the molecule is related to the potential of mean torque $U(\Omega)$ by

$$\mathbf{T} = i\boldsymbol{M}U(\Omega) \quad \text{(C2)}$$

In general, even in the Brownian motion limit, $\mathbf{R}(t)$ may be time dependent.[24,28] We have previously used two models in which $\mathbf{R}$ becomes time independent.[1] Case (1) is anisotropic rotation (e.g., molecular asymmetry) where the components of $\mathbf{R}$ in the molecular frame, which we will write as $\mathbf{R}_m$, are time independent. One quickly sees that it is $\mathbf{R}_m$ which appears in eq C1, so it becomes time independent. Case (2) is anisotropic viscosity, where the components of $\mathbf{R}$ in the lab frame, $\mathbf{R}_n$, are time independent. In this case, when we write $\boldsymbol{M}\cdot\mathbf{R}(t)\cdot\boldsymbol{M}$, the components of $\mathbf{R}(t)$ in the lab frame are rapidly fluctuating in time. It is therefore necessary to transform this dyadic scalar product (which can be written as the scalar product of two second rank irreducible tensors plus a scalar interaction, see below) into the lab frame as

$$\tilde{\Gamma}_\Omega = \boldsymbol{N}\cdot\mathbf{R}_n\cdot\boldsymbol{N} + [\boldsymbol{N}\cdot\mathbf{R}_n\cdot(\boldsymbol{N}U)]/2kT + \mathbf{T}_n\cdot\mathbf{R}_n\cdot\mathbf{T}_n/(2kT)^2 \quad \text{(C3)}$$

where

$$\mathbf{T}_n = i\boldsymbol{N}U(\Omega) \quad \text{(C4)}$$

The operator properties of $\boldsymbol{M}$ and $\boldsymbol{N}$ are given elsewhere.[1,38-40] Of course, for completely isotropic motion, we have $\boldsymbol{M}\cdot\mathbf{R}\cdot\boldsymbol{M} = R\boldsymbol{M}^2 = R\boldsymbol{N}^2 = \boldsymbol{N}\cdot R\cdot\boldsymbol{N}$, where R is the simple rotational diffusion coefficient.

The problem of combined anisotropic diffusion and anisotropic viscosity is more complex, because, in general, it is not possible to find a single axis system which renders $\mathbf{R}(t)$ time independent. However, in the spirit of the Brownian motion theory and models (1) and (2), one may obtain a simple solution for this case (3), by assuming $\mathbf{R}(t)$ can be decomposed into two parts: $\mathbf{R}(t) = \mathbf{R}_n + \mathbf{R}_m$, such that $\mathbf{R}_m$ is [as in case (1)] time independent in the molecular frame while $\mathbf{R}_n$ is [as in case (2)] time independent in the lab frame. Thus we obtain a time-independent diffusion operator (cf. eq C1 and C2) as

$$\tilde{\Gamma}_\Omega = \tilde{\Gamma}_{\Omega,n} + \tilde{\Gamma}_{\Omega,m} \quad \text{(C5)}$$

where $\tilde{\Gamma}_{\Omega,n}$ is given by eq C1 and $\tilde{\Gamma}_{\Omega,m}$ is given by eq C2. We will now assume axial symmetry of both $\mathbf{R}_n$ and $\mathbf{R}_m$ in their respective frames for the purpose of simplicity of discussion, although this is not necessary (see below). Then the normalized eigenfunctions of these operators in the absence of a restoring potential are the

$$\varphi^L_{KM}(\Omega) = \left(\frac{2L+1}{8\pi^2}\right)^{1/2}\boldsymbol{D}^L_{KM}(\Omega) \quad \text{(C6)}$$

and we obtain for $U(\Omega) = 0$

$$\tilde{\Gamma}_\Omega \phi^k_{Km}(\Omega) = (\boldsymbol{M}\cdot\mathbf{R}_m\cdot\boldsymbol{M} + \boldsymbol{N}\cdot\mathbf{R}_n\cdot\boldsymbol{N})\phi^k_{KM}(\Omega) = [(R_{m\perp} + R_{n\perp})L(L+1) + (R_{n\parallel} - R_{n\perp})M^2 + (R_{m\parallel} - R_{m\perp})K^2]\phi^k_{KM}(\Omega) \quad \text{(C7)}$$

In the presence of restoring potentials one has

$$\tilde{\Gamma}_\Omega = \boldsymbol{N}\cdot\mathbf{R}_n\cdot\boldsymbol{N} + \boldsymbol{M}\cdot\mathbf{R}_m\cdot\boldsymbol{M} - R_{n\perp}\hat{f}(\lambda,\rho\Omega) - f(R_{m\perp},R_{m\parallel},\lambda,\rho,\Omega) \quad \text{(C8)}$$

where $\hat{f}$ and f are given in I. [Note that we have previously used the notation $R_{m\perp} = R_\perp$, $R_{m\parallel} = R_\parallel$, $R_{n\perp} = \hat{R}_\perp$, and $R_{n\parallel} = \hat{R}_\parallel$, also one sees from I that $\hat{R}_\perp\hat{f}(\lambda,\rho,\Omega) = f(R_\perp\rightarrow\hat{R}_\perp,R_\parallel\rightarrow\hat{R}_\perp,\lambda,\rho,\Omega)$.]

The general situation for case (3) is best handled from the viewpoint of irreducible tensor notation. We illustrate by writing

$$\boldsymbol{M}\cdot\mathbf{R}_m\cdot\boldsymbol{M} = \sum_{\substack{L=0,2\\ p}} (-1)^p R_m^{(L,p)}(\boldsymbol{M}^2)^{(L,-p)} \quad \text{(C9)}$$

where the irreducible tensor components $R_m^{(L,p)}$ and $(\boldsymbol{M}^2)^{(L,-p)}$ are given by

$$R_m^{(0,0)} = -\frac{1}{\sqrt{3}}\,\mathrm{Tr}\,\mathbf{R}_m$$

$$R_m^{(2,0)} = \frac{1}{\sqrt{6}}(3R_{mzz} - \mathrm{Tr}\,\mathbf{R}_m) \quad \text{(C10)}$$

$$R_m^{(2,\pm1)} = \mp(R_{mzx} \pm iR_{myz})$$

$$R_m^{(2,\pm2)} = \tfrac{1}{2}(R_{mxx} - R_{myy} \pm 2iR_{xy})$$

$$(\boldsymbol{M}^2)^{(0,0)} = -\frac{1}{\sqrt{3}}\boldsymbol{M}^2$$

$$(\boldsymbol{M}^2)^{(2,0)} = \frac{1}{\sqrt{6}}(3\boldsymbol{M}_z^2 - \boldsymbol{M}^2) \quad \text{(C11)}$$

$$(\boldsymbol{M}^2)^{(2,\pm1)} = \frac{1}{\sqrt{2}}[\boldsymbol{M}_{\pm1}\boldsymbol{M}_z + \boldsymbol{M}_z\boldsymbol{M}_{\pm1}]$$

$$(\boldsymbol{M}^2)^{(2,\pm2)} = (\boldsymbol{M}_{\pm1})^2$$

where $\boldsymbol{M}_{\pm1} = \mp(1/\sqrt{2})(\boldsymbol{M}_x \pm i\boldsymbol{M}_y)$. An identical set of equations apply to $R_n^{(L,p)}$ and $(\boldsymbol{N}^2)^{(L,-p)}$. Then

$$\boldsymbol{N}\cdot\mathbf{R}_n\cdot\boldsymbol{N} + \boldsymbol{M}\cdot\mathbf{R}_m\cdot\boldsymbol{M} = \bar{R}\boldsymbol{M}^2 + \sum_p (-1)^p[R_n^{(2,p)}(\boldsymbol{N}^2)^{(2,-p)} + R_m^{(2,p)}(\boldsymbol{M}^2)^{(2,-p)}] \quad \text{(C12)}$$

where

$$\bar{R}\mathbf{M}^2 = \bar{R}\mathbf{N}^2 \quad \text{(C13)}$$

and

$$\bar{R} \equiv (1/3)\,\mathrm{Tr}\,\mathbf{R}(t) = 1/3(\mathrm{Tr}\,\mathbf{R}_m + \mathrm{Tr}\mathbf{R}_n)$$

The last two terms in eq C1 and in eq C2 can similarly be handled by irreducible tensor formalism.

Now eq C12 derives from the assumption of eq C5. However, the irreducible tensor form of eq C12 suggests that it may be possible to generalize this result so that $\bar{R}$ in eq C12 is simply the spherically symmetric part of $\mathbf{R}$, and it need not, in general, obey eq C13. [This generalization can also be carried out on the terms in $\tilde{\Gamma}_\Omega$ dependent upon $U(\Omega)$. One first expands $\mathbf{R}$ in terms of $\bar{R}$ and the components $R_n^{(2,p)}$ and $R_m^{(2,p)}$ in these terms.] The main requirements we place on the matrix $\mathbf{R}$ is that it be a real symmetric matrix with positive principal values in the coordinate system in which it is diagonal. Since the molecular and lab coordinates are fluctuating relative to each other, it is difficult in general to analyze for this latter condition. (It is immediately seen to be true for the form of eq C5.) Instead we can require that the eigenvalues of $\tilde{\Gamma}_\Omega$ all be real and positive. This guarantees that any nonequilibrium distribution of orientations decays to equilibrium. (Note, that $\tilde{\Gamma}_\Omega$ is defined so positive eigenvalues lead to negative exponential decay in time.) In that case, if we assume axial symmetry (i.e., only $R_m^{(2,0)}$ and $R_n^{(2,0)}$ are the only nonzero values of $R_m^{(2,p)}$ and $R_n^{(2,p)}$ then one finds that we require

$$\left[\bar{R} - \frac{2}{3\sqrt{6}}(R_m^{(2,0)} + R_n^{(2,0)})\right] > 0 \quad \text{(C14i)}$$

$$\left(\bar{R} + \frac{4}{3\sqrt{6}}R_m^{(2,0)}\right) > 0 \quad \text{(C14ii)}$$

$$\left(\bar{R} + \frac{4}{3\sqrt{6}}R_n^{(2,0)}\right) > 0 \quad \text{(C14iii)}$$

$$\left[\bar{R} + \frac{4}{3\sqrt{6}}(R_m^{(2,0)} + R_n^{(2,0)})\right] > 0 \quad \text{(C14iv)}$$

This set of requirements is less restrictive than eq C5. In the case where $R_n^{(2,0)} = 0$, the choice of $\bar{R} = 1/3(R_{m\parallel} + 2R_{m\perp})$ and $(2/\sqrt{6})R_m^{(2,0)} = (R_{m\parallel} - R_{m\perp})$ leads to the expected requirements that $R_{m\perp} > 0$ [from (i)] and that $R_{m\perp\perp} > 0$ [from (ii)].

Appendix D. Brownian vs. Strong-Jump Reorientation and Angular-Dependent Line Widths

In this work we have used Brownian motion models as a starting point for our analysis and the introduced non-Brownian corrections. Strong jump models are often used because of the simplicity of the results, although there is not very good theoretical justification for their use. Here we compare predictions of angular-dependent line widths for isotropic Brownian vs. strong jump models. The zero-frequency spectral densities for Brownian motion are conveniently fit to a polynomial in $\langle \boldsymbol{D}_{00}^2(\Omega)\rangle$ for axial symmetry. Such a table was given in ref 25, based on calculations of Polnaszek. These calculations have been refined somewhat, and the new fits appear in Table VII. With the exception of $J_{11}(0)$, they yield slightly better fits, but the new $J_{11}(0)$ do involve a significant numerical correction. The results in Table VII and Table I of ref 25 or the more general form of Table VI [along with the strong-collision form of $J^{(1)}_{KM}(0) = \kappa(K,M)\tau_R$][25] were used to compare the two models in Figure 20. One finds that for weak ordering, appropriate for PD-Tempone (e.g., the S_A phase of 8CB), the predictions from the two models are nearly the same. However, for strong ordering, appropriate for CSL, there are significant differences in the angular dependence predicted by the two models. (The results for strong ordering are only approximate for both models because we did not correct for the effect of the changing nuclear spin quantization axis as θ is varied.)[28]

We thus conclude that it is not necessary to distinguish between different jump models in properly analyzing the motional-narrowing results for weakly ordered PD-Tempone.

References and Notes

(1) C. F. Polnaszek and J. H. Freed, *J. Phys. Chem.*, **79**, 2283 (1975), referred to as I.
(2) K. V. S. Rao, C. F. Polnaszek, and J. H. Freed, *J. Phys. Chem.*, **81**, 449 (1977), referred to as II.
(3) (a) G. R. Luckhurst and M. Setaka, *Mol. Cryst. Liq. Cryst.*, **19**, 179 (1972); (b) G. R. Luckhurst, M. Setaka, and C. Zannoni, *Mol. Phys.*, **28**, 49 (1974).

(4) (a) F. Pusnick, M. Schara, and M. Sentjurc, *J. Phys.* (*Paris*), **36**, 665 (1975); (b) F. Pusnick and M. Schara, *Chem. Phys. Lett.*, **37**, 106 (1976).
(5) See also the NMR study of Z. Luz and S. Meiboom, *J. Chem. Phys.*, **59**, 275 (1973).
(6) (a) G. R. Luckhurst and A. Sanson, *Mol. Phys.*, **24**, 1297 (1972); (b) G. R. Luckhurst, M. Ptak, and A. Sanson, *J. Chem. Soc., Faraday Trans. 2*, **69**, 1752 (1973).
(7) D. Sy and M. Ptak, *Mol. Cryst. Liq. Cryst.*, **39**, 53 (1977). These authors used small nitroxide probes as well as large ones, but they did not study spin relaxation.
(8) J. S. Hwang, R. P. Mason, L. P. Hwang and J. H. Freed, *J. Phys. Chem.*, **79**, 489 (1975).
(9) S. Zager, K. V. S. Rao, and J. H. Freed, to be published.
(10) J. S. Hwang, K. V. S. Rao, and J. H. Freed, *J. Phys. Chem.*, **80**, 1490 (1976).
(11) K. V. S. Rao, J. S. Hwang, and J. H. Freed, *Phys. Rev. Lett.*, **37**, 515 (1976).
(12) J. A. Murphy, *Mol. Cryst. Liq. Cryst.*, **22**, 133 (1973).
(13) E. G. Rozantsev, "Free Nitroxyl Radicals", Plenum Press, New York, N.Y., 1970.
(14) C. Reichardt, *Angew. Chem., Int. Ed. Engl.*, **4**, 29 (1965).
(15) We thank Professor M. Goldstein for calling these methods to our attention.
(16) (a) J. Seelig, H. Limacher, and P. Bader, *J. Am. Chem. Soc.*, **94**, 6364 (1972); see also Chapter 10 of "Spin-Labelling: Theory and Applications", L. J. Berliner, Ed., Academic Press, New York, 1976. (b) O. H. Griffith et al., *J. Membr. Biol.*, **15**, 159 (1974); see also Chapter 12 of "Spin-Labelling: Theory and Applications", L. J. Berliner, Ed., Academic Press, New York, 1976.
(17) However, see recent work of M. C. R. Symons, *Pure Appl. Chem.*, **49**, 13 (1977); also Y. Y. Lim, E. A. Smith, and M. C. R. Symons, *J. Chem. Soc., Faraday Trans 1*, **72**, 2876 (1976); S. E. Jackson, E. A. Smith, and M. C. R. Symons, *ibid.*, **74**, 562 (1978).
(18) G. R. Luckhurst and G. W. Gray, Ed., "The Molecular Physics of Liquid Crystals", Lectures at NATO Advanced Institute, 1977, to be published. See chapters by G. W. Gray, A. J. Leadbetter, and J. Doucet, and references therein.
(19) P. E. Cladis, R. K. Bogardus, W. B. Daniels, and G. N. Taylor, *Phys. Rev. Lett.*, **39**, 720 (1977).
(20) E. B. Priestley et al., Ed., "Introduction to Liquid Crystals", Plenum Press, New York, 1975, p 194.
(21) (a) G. K. Fraenkel, *J. Chem. Phys.*, **42**, 4275 (1965); (b) J. H. Freed in "Electron-Spin Relaxation in Liquids", Plenum Press, New York, 1972, Chapter VIII.
(22) The actual analysis of this E_a may be complicated by the increased interpenetration of the hydrocarbon chains from adjacent smectic layers as the layer spacing decreases with decreasing temperature. In fact in a fluctuating torque model,[8] where $\tau_R = V^2\tau_M/6IkT$ (see below), one could postulate that the net instantaneous torque experienced by the PD-Tempone is reduced as the flexible end chains interpenetrate more and their random torque components tend to average each other out more. Thus one would have $V^2 = V_0^2 e^{-E_v/kT}$ while $\tau_M = \tau_{M_0} e^{E_a'/kT}$ with $E_a = E_a' - E_v$.
(23) In fact, while we have suggested in footnote 22 that V^2 could be decreasing with decreasing temperature, the slowly fluctuating torque components that contribute to SRLS may be expected to increase; see discussion of SmB.
(24) L. P. Hwang and J. H. Freed, *J. Chem. Phys.*, **63**, 118 (1975).
(25) J. H. Freed, *J. Chem. Phys.*, **66**, 4183 (1977).
(26) G. R. Luckhurst and R. N. Yeates, *J. Chem. Soc., Faraday Trans. 2*, **72**, 996 (1976).
(27) One need only substitute the angular-dependent spectral densities given (for axially symmetric ordering) by eq 7.17 and 7.18 of I into eq 2.31 of I. Equations 7.17 and 7.18 of I are readily generalized to the case of nonaxial symmetry needed for this work, e.g.

$$\hat{\kappa}(2,K,K',\omega,\theta) = (1/5)D_{K,K'} + (2/7)P_2(\cos\theta)E_{K,K'} + (6/35)P_4(\cos\theta)F_{K,K'} \text{ etc.}$$

with $D_{K,K'} \equiv \kappa(2,K,K',0,\omega) + 2\kappa(2,K,K',1,\omega) + 2\kappa(2,K,K',2,\omega)$, etc. Note that $J_{K,K'M}(\omega) \equiv \text{Re } \kappa(2,K,K',M,\omega)$.
(28) It is not necessary to correct for the effect on the line widths of nuclear spin quantization along an axis other than the magnetic field, which can be of some importance in the tilt experiments, as Luckhurst and Zannoni [*Proc. R. Soc. London, Ser. A*, **353**, 87 (1977)] have shown, because one finds that for the weak ordering of PD-Tempone such corrections are negligible. (Note that in a slow-tumbling theory, cf. I, such effects would be automatically included).
(29) C. F. Polnaszek, Ph.D. Thesis, Cornell University, 1975.
(30) S. A. Brooks, G. R. Luckhurst, G. F. Pedulli, and J. Roberts, *J. Chem. Soc., Faraday Trans. 2*, **72**, 651 (1976), discussed line shape asymmetries for VO^{+2}(acac) in the nematic phase in terms of static director fluctuations. However, such vanadyl line shapes are now known to arise from slow-tumbling effects [cf. G. V. Bruno, J. K. Harrington, and M. P. Eastman, *J. Phys. Chem.*, **81**, 1111 (1977); R. F. Campbell and J. H. Freed, to be published].
(31) H. Schindler and J. Seelig, *J. Chem. Phys.*, **59**, 1841 (1973); **61**, 2946 (1974), discuss lyotropics.
(32) L. J. Libertini, C. A. Burke, P. C. Jost, O. H. Griffith, *J. Mag. Reson.*, **15**, 460 (1974), discussed phospholipids.
(33) B. J. Gaffney and H. M. McConnell, *J. Mag. Reson.*, **16**, 1 (1974). These authors also consider a distribution function, which in our notation is $P_{eq}(\Psi) = Ne^{-\alpha\theta'^2-\beta\varphi'^2}$, for purposes of discussing smectic-C-like properties of phospholipids in a magnetic field.
(34) P. G. de Gennes, "The Physics of Liquid Crystals", Oxford University Press, New York, 1974.
(35) M. J. Stephen and J. S. Straley, *Rev. Mod. Phys.*, **46**, 617 (1974).
(36) N. A. Clark and P. S. Pershan, *Phys. Rev. Lett.*, **30**, 3 (1973); R. Ribotta, G. Durand, and J. D. Litster, *Solid State Commun.*, **12**, 27 (1973).
(37) (a) In preliminary studies, we have found that, when very thin samples of PD-tempone in (40,8) are prepared between glass plates, the PD-tempone soon plates out on the surface of the plates. The other problem is to degass such samples to obtain good spectral resolution. Further work on thse problems is continuing. (b) P. S. Pershan and J. Prost, *J. Appl. Phys.*, **46**, 2343 (1975).
(38) L. D. Favro in "Fluctuation Phenomena in Solids", R. E. Burgess, Ed., Academic Press, New York, 1965, p 79.
(39) J. H. Freed, *J. Chem. Phys.*, **41**, 2077 (1964).
(40) C. F. Polnaszek, G. V. Bruno, and J. H. Freed, *J. Chem. Phys.*, **58**, 3185 (1973).